ADAPTIVE COARSE SPACES FOR FETI-DP IN THREE DIMENSIONS[‡]

AXEL KLAWONN*, MARTIN KÜHN*, AND OLIVER RHEINBACH†

July 19, 2016

Abstract. An adaptive coarse space approach including a condition number bound for FETI-DP methods applied to three dimensional problems with coefficient jumps inside subdomains and across subdomain boundaries is presented. The approach is based on a known adaptive coarse space approach enriched by a small number of additional local edge eigenvalue problems. These edge eigenvalue problems serve to make the method robust and permit a condition number bound which depends only on the tolerance of the local eigenvalue problems and some properties of the domain decomposition. The introductions of the edge eigenvalue problems thus turns a well-known condition number indicator for FETI-DP and BDDC methods into a condition number estimate. Numerical results are presented for linear elasticity and heterogeneous materials supporting our theoretical findings. The problems considered include those with random coefficients and almost incompressible material components.

Key words. FETI-DP, eigenvalue problem, coarse space, domain decomposition, adaptive, BDDC, elasticity, almost incompressible

1. Introduction. Second-order elliptic equations with discontinuous coefficents often yield very ill conditioned stiffness matrices when discretized by finite elements. Examples are diffusion problems or elasticity problems with materials having large discontinuities in the diffusion coefficients and the Young modulus, respectively. Almost incompressible components can be also a source of ill-conditioning in the case of linear elasticity. These sources of ill-conditioning can lead to a severe deterioration of the convergence rate of iterative methods that are used to solve the resulting linear system. Here, we will consider domain decomposition algorithms as iterative solution methods. A heterogeneous material can lead to coefficient jumps accross and along subdomain boundaries, especially when an automatic graph partitioner is used to create the domain decomposition. Certain problems with special coefficient distributions, such as constant coefficients on subdomains, can then still be handled by using special scalings; see, e.g., [53, 37, 21, 35, 50, 1]. However, there are many cases when this is not sufficient and an augmentation of the coarse space is needed to ensure a small condition number and the convergence of the iterative scheme within a reasonable number of iterations. An additional approach to enhance the coarse space of the domain decomposition algorithm is to first solve local (generalized) eigenvalue problems and then incorporate these eigenvectors appropriately into the coarse space. This strategy is mostly based on certain user-given tolerances for the eigenvalue problems which determine the amount of extra work to be carried out in order to obtain good convergence properties. These adaptive strategies exist for many kinds of domain decomposition algorithms such as overlapping Schwarz, FETI/BDD (Finite Element Tearing and Interconnecting/Balancing Domain Decomposition), or FETI-DP/BDDC (Dual Pri-

*Mathematisches Institut, Universität zu Köln, Weyertal 86-90, 50931 Köln, Germany; {axel.klawonn,martin.kuehn}@uni-koeln.de.

†Technische Universität Bergakademie Freiberg, Fakultät für Mathematik und Informatik, Institut für Numerische Mathematik und Optimierung, 09596 Freiberg, Germany; oliver.rheinbach@math.tu-freiberg.de.

‡Some preliminary, partial results without proofs will appear in the proceedings of the 23rd International Conference on Domain Decomposition Methods [28]. The present article contains a significantly enhanced and extended version, including complete proofs.

mal Finite Element Tearing and Interconnecting/Balancing Domain Decomposition by Constraints); see, e.g., [4, 5, 15, 16, 9, 60, 61, 12, 26, 31, 44, 45, 7, 2, 48, 6, 49, 29]. In [29], a very brief overview on adaptive coarse spaces for domain decomposition methods can be found.

The approach presented in this paper is based on the adaptive coarse space from [44] for FETI-DP. For two dimensions, the first proof for the approach from [44] was published in [32]. For three dimensions, Theorem 6.1, presented in the present paper, provides the first proof for an enhanced approach based on [44]; cf. the introduction of our coarse space in Section 5. Let us note that some of our results have been presented at the 23rd International Conference on Domain Decomposition Methods (DD23) [27]. At the same conference, other adaptive approaches were also announced in the talks of C. R. Dohrmann [8], H. H. Kim [24], and O. B. Widlund [63]. After the DD23 conference, the new approaches for adaptive BDDC and FETI-DP were made public in several technical reports [30, 2, 48, 6], and, very recently in [25]. Another very recent technical report gave an overview on adaptive BDDC; see [49]. The technical report version of the present paper [30] contained the first publically available proof in three dimensions for the P_D-based family of approaches [44, 7], which use very localized eigenvalue problems.

For FETI instead of FETI-DP, a different algorithm was introduced and analyzed in [61]. This coarse space was originally established for overlapping Schwarz methods (see [59, 60]) and then transferred to BDD and FETI.

The coarse space [44] was already used extensively also in 3D (without the edge eigenvalue problems proposed in this paper), see [45], also to create a parallel adaptive multilevel BDDC [57]. But no rigorous condition number bound had existed, although a heuristic indicator was derived in [44]. Recently, in [32], proofs were given in detail for the algorithms of [44] and [7] in two dimensions, and they were both compared to the approach in [31]. In [32], the authors also presented a modification of [7] that allowed other scalings than deluxe scaling. The paper presented here now provides the theory for the three dimensional case by adding edge eigenvalue problems to the classic approach [44], which used face eigenvalues, only.

Our extension of the coarse space designed by the authors of [44] consists of adding eigenvalue problems on edges belonging to more than three subdomains which have to be solved in addition to the face eigenvalue problems. Then, we can prove a robust condition number bound for the preconditioned FETI-DP operator. This bound depends on a user-given tolerance TOL; see Theorem 6.2. Note that, when an automatic mesh partitioner is used in 3D, these edges (with a multiplicity of four or larger) are rare (in practice a few percent or less [52]), as border quadrangle are rare on the globe. However, without the edge eigenvalue problems, a few bad eigenvalues resulting from these edges can spoil the convergence of the Krylov solver; see, e.g., Table 8.2.

We will provide our bound and its proof for three dimensional elasticity using deflation techniques although other implementations of the coarse space are also possible. We will also discuss the cost and necessity of these additional eigenvalue problems. Our results are of equal interest for adaptive BDDC methods [45].

The remainder of the paper is organized as follows: In Section 2, we introduce the model problem, mention the corresponding finite element discretizations that will be used and outline the domain decomposition approach. Sections 3 and 4 give a short introduction to FETI-DP methods, scalings, preconditioners and deflation (also known as projector preconditioning) and balancing techniques. In Section 5, we will

explain how the operators necessary for computing constraints are established and how the latter are obtained. Our approach starts with the adaptive coarse space of [44] and adds constraints from supplementary eigenvalue problems. Based on the new adaptively computed coarse space, in Section 6, we will give the proof for the bound on the condition number as mentioned. In Section 7 we outline some ideas on how to reduce the number of eigenvalue problems and constraints. Section 8 will provide several tests of compressible and almost incompressible elasticity and compare the algorithms proposed by [44] with the modified coarse space presented here. Additionally, at the end of the section, we will test an approach to reduce the number of eigenvalue problems. Eventually, in Section 9, we will draw conclusions from our theory and simulations and provide advice when the respective coarse space should be used.

2. Model problem and geometry. Let $\Omega \subset \mathbb{R}^d$, $d = 2, 3$ be a bounded polyhedral domain, let $\partial\Omega_D \subset \partial\Omega$ be a closed subset of nonvanishing measure and let $\partial\Omega_N := \partial\Omega \setminus \partial\Omega_D$. In addition, we define the Sobolev space $H^1_0(\Omega, \partial\Omega_D)^d := \{v \in H^1(\Omega)^d : v = 0 \text{ on } \partial\Omega_D\}$, Young's modulus $\mathrm{E}(x) > 0$, and Poisson's ratio $0 < \nu(x) < \frac{1}{2}$ for all $x \in \Omega$. We consider the variational formulation of compressible linear elasticity: Find $u \in H^1_0(\Omega, \partial\Omega_D)^d$, such that

$$a(u, v) = F(v) \quad \forall v \in H^1_0(\Omega, \partial\Omega_D)^d, \tag{2.1}$$

with $a(u, v) := \int_\Omega 2\mu\varepsilon(u) : \varepsilon(v)\mathrm{d}x + \int_\Omega \lambda \mathrm{div}(u)\mathrm{div}(v)\mathrm{d}x$ and $F(v) := \int_\Omega f \cdot v\mathrm{d}x + \int_{\partial\Omega_N} g \cdot v\mathrm{d}s$. Here, the Lamé constants λ and μ can be computed from E and ν as $\lambda = \frac{\mathrm{E}\nu}{(1+\nu)(1-2\nu)}$, $\mu = \frac{\mathrm{E}}{2(1+\nu)}$. The product $\varepsilon(u) : \varepsilon(v)$ of the linearized strain tensor $\varepsilon(v)$ with $\varepsilon_{ij}(v) = \frac{1}{2}(\partial v_i/\partial x_j + \partial v_j/\partial x_i)$ is given by $\varepsilon(u) : \varepsilon(v) = \sum_{i,j=1}^N \varepsilon_{ij}(u)\varepsilon_{ij}(v)$. The functions $f : \Omega \to \mathbb{R}^d$ and $g : \partial\Omega_N \to \mathbb{R}^d$ are given volume and surface forces, respectively, prescribed on Ω and the Neumann boundary $\partial\Omega_N$.

With Poisson's ratio ν approximating 0.5, we speak of almost incompressible elasticity. For almost incompressible elasticity locking phenomena can occur for the standard formulation and therefore the pressure variable $p := \lambda \mathrm{div}(u)$ is introduced. Then, we derive the weak form of the mixed formulation in (u, p). Special care has to be taken when chosing the finite elements for solving the mixed formulation. It has to be ensured that the chosen finite elements fulfill the discrete Ladyženskaya-Babuška-Brezzi condition to remain stable.

We decompose Ω into N nonoverlapping subdomains Ω_i, $i = 1, \ldots, N$ where each Ω_i is the union of shape regular tetrahedral or, in almost incompressible cases, brick elements of diameter $\mathcal{O}(h)$. The diameter of a subdomain is denoted by H_i or, generically, by H. Furthermore, we define the interface Γ as the set of values that belong to at least two subdomains and require that finite element nodes of neighboring subdomains match across the interface. The interface in three dimensions consists of vertices, edges, and faces, defined as in [38]. Edges and faces are considered as open sets. We will denote a face between the two subdomains Ω_i and Ω_j by $\mathcal{F}^{ij}$, an edge between Ω_i, Ω_j, Ω_l and maybe other subdomains by $\mathcal{E}^{il}$ and a vertex of Ω_i touching several subdomains by $\mathcal{V}^{ik}$. We further define Γ_h and $\partial\Omega_{i,h}$ as the set of finite element nodes on Γ and $\partial\Omega_i$, respectively. Eventually, for an arbitrary face $\mathcal{F}$ and an arbitrary edge $\mathcal{E}$ we introduce the standard finite element cutoff functions $\theta_\mathcal{F}$ and $\theta_\mathcal{E}$, which are equal to 1 on $\mathcal{F}$ and $\mathcal{E}$, respectively, and are zero otherwise.

For the case of compressible linear elasticity, we use $\mathcal{P}_1$ conforming finite elements. If Poisson's ratio ν approaches the incompressible limit, we take $\mathcal{Q}_2 - \mathcal{P}_0$ conforming

finite elements which are inf-sup stable. In our experiments, we will statically condensate the pressure variable elementwise. The space of our finite elements on Ω_i, consisting of either standard piecewise linear finite elements or statically condensated $\mathcal{Q}_2 - \mathcal{P}_0$ finite elements, is denoted by $W^h(\Omega_i)$. In both cases the finite element functions vanish on $\partial\Omega_D$. For a part of the interface $\Gamma' \subset \Gamma$ with nonvanishing measure we define the finite element trace space $W^h(\Gamma')$ and, in particular, $W_i := W^h(\partial\Omega_i)$. Finally, we define $W := \Pi_{i=1}^N W_i$ and denote by $\widehat{W} \subset W$ the space of functions in W that are continuous on Γ.

3. FETI-DP Method. In this section, we will briefly review the standard FETI-DP algorithm. For a more detailed description on FETI-DP, see, e.g., [14, 13, 62], and, especially in combination with linear elasticity, [38].

For every subdomain $i = 1, \ldots, N$ we compute the the local stiffness matrix $K^{(i)}$ and the right hand side $f^{(i)}$. We subdivide the set of degrees of freedom into interior I, dual Δ, and primal Π degrees of freedom. Interior degrees of freedom will belong to nodes in the interior of subdomains and on the Dirichlet boundary $\partial\Omega_D$ while dual and primal degrees of freedom belong to nodes on the interface Γ. The corresponding variables on $\overline{\Omega}_i$ will be denoted by $u_I^{(i)}$, $u_\Delta^{(i)}$, and $u_\Pi^{(i)}$. The choice of Π will determine the initial coarse space. We will set all vertices according to the definition of [38, Def. 3.1] (see also [34]) primal and require that there are at least two primal nodes on every edge $\mathcal{E}^{il}$. Moreover, if $\mathcal{E}^{il}$ is a nonstraight edge, we set a third one primal, that does not lie on a straight line between the other two. This only is an issue for irregular decompositions of Ω and the necessity of this will be explained in more detail in Remark 1; see Section 5. Using the notation introduced before, for theoretical purpose, we can assume the following partitioning

$$K^{(i)} = \begin{bmatrix} K_{II}^{(i)} & K_{\Delta I}^{(i)T} & K_{\Pi I}^{(i)T} \\ K_{\Delta I}^{(i)} & K_{\Delta\Delta}^{(i)} & K_{\Pi\Delta}^{(i)T} \\ K_{\Pi I}^{(i)} & K_{\Pi\Delta}^{(i)} & K_{\Pi\Pi}^{(i)} \end{bmatrix}, u^{(i)} = \begin{bmatrix} u_I^{(i)} \\ u_\Delta^{(i)} \\ u_\Pi^{(i)} \end{bmatrix}, \text{ and } f^{(i)} = \begin{bmatrix} f_I^{(i)} \\ f_\Delta^{(i)} \\ f_\Pi^{(i)} \end{bmatrix}.$$

We also introduce the block diagonal matrices

$$K_{II} := \operatorname{diag}_{i=1}^N K_{II}^{(i)}, K_{\Delta\Delta} := \operatorname{diag}_{i=1}^N K_{\Delta\Delta}^{(i)}, \text{ and } K_{\Pi\Pi} := \operatorname{diag}_{i=1}^N K_{\Pi\Pi}^{(i)}.$$

Combining the index sets I and Δ to the index set B leads to

$$K_{BB}^{(i)} := \begin{bmatrix} K_{II}^{(i)} & K_{\Delta I}^{(i)T} \\ K_{\Delta I}^{(i)} & K_{\Delta\Delta}^{(i)} \end{bmatrix}, K_{\Pi B}^{(i)} := \begin{bmatrix} K_{\Pi I}^{(i)} K_{\Pi\Delta}^{(i)} \end{bmatrix} \text{ and } f_B^{(i)} := \begin{bmatrix} f_I^{(i)T} f_\Delta^{(i)T} \end{bmatrix}^T$$

as well as to the block structures

$$K_{BB} := \operatorname{diag}_{i=1}^N K_{BB}^{(i)}, u_B := \begin{bmatrix} u_B^{(1)T}, \ldots, u_B^{(N)T} \end{bmatrix}^T, \text{ and } f_B := \begin{bmatrix} f_B^{(1)T}, \ldots, f_B^{(N)T} \end{bmatrix}^T.$$

A union of the index sets Δ and Π results in the index set Γ and the matrices $K_{\Gamma\Gamma}^{(i)}$ and $K_{\Gamma I}^{(i)}$ which will be needed for our preconditioner and generalized eigenvalue problems. Furthermore, we need partial assembly operators $R_\Pi^{(i)T}$ and $R_\Pi^T = \begin{bmatrix} R_\Pi^{(1)T}, \ldots, R_\Pi^{(N)T} \end{bmatrix}$ so that R_Π^T assembles the variables $u_\Pi^{(i)}$, $i = 1, \ldots, N$, associated with primal degrees

of freedom. The space of functions that are continuous in the primal variables will be denoted by $\widetilde{W} \subset W$. We introduce

$$\widetilde{K}_{\Pi\Pi} = \sum_{i=1}^{N} R_{\Pi}^{(i)T} K_{\Pi\Pi}^{(i)} R_{\Pi}^{(i)}, \widetilde{K}_{\Pi B} = \left[R_{\Pi}^{(1)T} K_{\Pi B}^{(1)}, \ldots, R_{\Pi}^{(N)T} K_{\Pi B}^{(N)} \right], \widetilde{f} = \left[f_B^T, (\sum_{i=1}^{N} R_{\Pi}^{(i)T} f_{\Pi}^{(i)})^T \right]^T,$$

and the jump operator $B = \left[B^{(1)}, \ldots, B^{(N)} \right]$ with $Bu = 0$ for $u \in \widehat{W}$. This yields

$$\begin{bmatrix} \widetilde{K} & B^T \\ B & 0 \end{bmatrix} \begin{bmatrix} \widetilde{u} \\ \lambda \end{bmatrix} = \begin{bmatrix} \widetilde{f} \\ 0 \end{bmatrix}.$$

Here, $\widetilde{K}$ and $\widetilde{f}$ are of the form

$$\widetilde{K} = \begin{bmatrix} K_{BB} & \widetilde{K}_{\Pi B}^T \\ \widetilde{K}_{\Pi B} & \widetilde{K}_{\Pi\Pi} \end{bmatrix} \text{ and } \widetilde{f} = \begin{bmatrix} f_B \\ \widetilde{f}_{\Pi} \end{bmatrix}.$$

Assuming invertibility of K_{BB}, we can form the FETI-DP coarse operator

$$\widetilde{S}_{\Pi\Pi} = \widetilde{K}_{\Pi\Pi} - \widetilde{K}_{\Pi B} K_{BB}^{-1} \widetilde{K}_{\Pi B}^T. \tag{3.1}$$

After a second elimination step, we obtain the FETI-DP system $F\lambda = d$ where

$$\begin{aligned} F &= B_B K_{BB}^{-1} B_B^T + B_B K_{BB}^{-1} \widetilde{K}_{\Pi B}^T \widetilde{S}_{\Pi\Pi}^{-1} \widetilde{K}_{\Pi B} K_{BB}^{-1} B_B^T, \\ d &= B_B K_{BB}^{-1} f_B + B_B K_{BB}^{-1} \widetilde{K}_{\Pi B}^T \widetilde{S}_{\Pi\Pi}^{-1} \left(\left(\sum_{i=1}^{N} R_{\Pi}^{(i)T} f_{\Pi}^{(i)} \right) - \widetilde{K}_{\Pi B} K_{BB}^{-1} f_B \right). \end{aligned}$$

Then, the FETI-DP system can be solved by the preconditioned conjugate gradients (PCG) algorithm. The appearance of $\widetilde{S}_{\Pi\Pi}^{-1}$ in F provides a coarse problem. This coarse problem is determined by the size of the primal degrees of freedom and should accelerate convergence.

Other more advanced coarse spaces based on averages or first-order moments over edges or faces could be used and implemented using a transformation of basis; see, e.g., [14, 39, 38, 43, 35]. Here, for simplicity, we will only consider primal vertex constraints as an initial coarse space. We will then use adaptive constraints to reduce the condition number as described in the next section. This will allow us to prove the condition number bound which we will present in Section 6 for problems with coefficient jumps in 3D.

Next, we introduce the standard Dirichlet preconditioner M_D^{-1}. The extension and restriction operators R_Γ^T and R_Γ from and onto Γ consist of zeros and ones. R_Γ^T extends a vector by zero onto Γ while R_Γ restricts a vector correspondingly by removing interior variables. For $x \in \Gamma_h \cap \partial\Omega_{i,h}$ let $\mathcal{N}_x$ be the set of indices of subdomains that have x on their boundaries. Then, we define the nodal coefficient evaluation $\widehat{\rho}_i(x) := \sup_{x \in \text{supp}(\varphi_x) \cap \Omega_i} \rho(x)$, where φ_x is the nodal finite element function at x, $\text{supp}(\varphi_x)$ its support, and $\rho(x)$ is the coefficient value at x. For linear elasticity, $\rho(x) = \text{E}(x)$, i.e., we use the Young Modulus. Let Ω_j share a face or an edge with Ω_i and $x \in \partial\Omega_{i,h} \cap \partial\Omega_{j,h}$, then, the corresponding nonzero row of $B^{(j)}$ is scaled by $\delta_i^\dagger(x) := \widehat{\rho}_i(x) / \sum_{k \in \mathcal{N}_x} \widehat{\rho}_k(x)$ and vice versa; see, e.g., [54, 37, 62]. This defines the local scaling matrix D_j and the scaled jump operator

$B_D = \left[B_D^{(1)}, \ldots, B_D^{(N)}\right] = \left[D_1 B^{(1)}, \ldots, D_N B^{(N)}\right]$. The standard Dirichlet preconditioner is now given by

$$M_D^{-1} := B_D R_\Gamma^T S R_\Gamma B_D^T,$$

where $S := \operatorname{diag}_{i=1}^N S^{(i)}$ and $S^{(i)}$ is the local Schur complement after elimination of the interior variables from $K^{(i)}$, that is

$$S^{(i)} := K_{\Gamma\Gamma}^{(i)} - K_{\Gamma I}^{(i)} \left(K_{II}^{(i)}\right)^{-1} K_{\Gamma I}^{(i),T}.$$

Let us remark that there are other choices for the scaling available in the literature (see, e.g., [53, 21, 1]), but we restrict ourselves in the numerical results presented in Section 8 to the case mentioned above and referred to as ρ- or patch-ρ-scaling; cf., [35, 50].

4. Deflation and Balancing. In this section, we briefly explain the deflation and the balancing approach. Deflation [47] is also known as projector preconditioning [10]. These approaches provides a mechanism to enhance the coarse space by additional constraints. Other possibilities are a transformation of basis or optional Lagrange multipliers; see, e.g., [34, 38] and [20, 38], respectively. For a short introduction to deflation and balancing, especially in the context of FETI-DP and domain decomposition methods, see [47, 10, 11, 46, 36, 22] and the references therein.

In the following for a matrix A, by A^+ we denote an arbitrary pseudoinverse satisfying $AA^+A = A$ and $A^+AA^+ = A^+$.

The following description is based on [36] extended to the case of a semidefinite matrix F. Let $U = (u_1, \ldots, u_k)$ be given as the matrix where the constraints are stored as columns. Then, we define

$$P := U(U^T F U)^+ U^T F.$$

We have $\operatorname{range} P = \operatorname{range}(U(U^T F U)^+)$ and $\ker P = \ker(U^T F U)^+ U^T F)$. Next, we multiply the FETI-DP system by $(I-P)^T$, which yields the deflated system

$$(I-P)^T F \lambda = (I-P)^T d. \tag{4.1}$$

The deflated system is consistent. Moreover, $\operatorname{range} U \subset \ker((I-P)^T F)$, and therefore $\operatorname{range}(F(I-P)) \subset \ker U^T$ remains valid also for a semidefinite matrix F. Since $(I-P)^T$ is also a projection, we can show that

$$(I-P)^T F = F(I-P) = (I-P)^T F (I-P).$$

Therefore, only components of the dual variable in $\operatorname{range}(I-P)$ are relevant to the construction of the Krylov spaces. By λ^* we denote the solution of the original system $F\lambda = d$, which is unique only up to an element in $\ker B^T$. Let $\hat{\lambda} \in \operatorname{range}(I-P)$ be a solution of (4.1). Then, $\hat{\lambda}$ is identical to $(I-P)\lambda^*$ up to an element in $\ker B^T$. We have the decomposition

$$\lambda^* = P\lambda^* + (I-P)\lambda^* =: \bar{\lambda} + (I-P)\lambda^*,$$

where $\bar{\lambda}$ can be expressed by $\bar{\lambda} = P\lambda^* = U(U^T F U)^+ U^T F F^+ F \lambda^* = P F^+ d$. Since $B^T(I-P)\lambda^* = B^T\hat{\lambda}$, we can then show that the solution in terms of the displacements does not change if $(I-P)\lambda^*$ is replaced by $\hat{\lambda}$, i.e.,

$$u_\Delta = \widetilde{S}^{-1}\left(\widetilde{f}_\Delta - B^T\lambda^*\right) = \widetilde{S}^{-1}\left(\widetilde{f}_\Delta - B^T(\bar{\lambda} + \hat{\lambda})\right).$$

Preconditioning the resulting system of equations by the Dirichlet preconditioner M_D^{-1} gives

$$M_D^{-1}(I-P)^T F\lambda = M_D^{-1}(I-P)^T d.$$

Another multiplication with $I-P$ from the left gives the new symmetric preconditioner $M_{PP}^{-1} := (I-P)M_D^{-1}(I-P)^T$ which can also be denoted deflation preconditioner. As shown in [36, Theorem 6.1], we do not change the nonzero eigenvalues of the former left hand side when multiplying with $I-P$. Therefore, the deflated problem reads: Find $\lambda \in \text{range}\,(I-P)$, such that

$$M_{PP}^{-1} F\lambda = M_{PP}^{-1} d.$$

Instead of computing $\bar{\lambda}$ a posteriori, the computation can be included into each iteration. This leads to the balancing preconditioner $\widehat{M}_{BP}^{-1} := M_{PP}^{-1} + PF^+$. Although the balancing preconditioner for a semidefinite matrix F is then of the form $\widehat{M}_{BP}^{-1} = M_{PP}^{-1} + U(U^TFU)^+U^TFF^+$ we can equivalently use

$$M_{BP}^{-1} = M_{PP}^{-1} + U(U^TFU)^+U^T$$

since it will be applied to $F\lambda = d$. Let us note that the Theorems 6.2 and 6.3 in [36] can be proven for a semidefinite matrix F by replacing F^{-1} by F^+ and by following the arguments given in [36]. As a result, we obtain that the eigenvalues of $M_{BP}^{-1}F$ and $M_{PP}^{-1}F$ are essentially the same. In order to provide a condition number bound for the deflation and the balancing approach let us first assume that a standard Rayleigh quotient estimate for the $P_D := B_D^TB$ operator is given, i.e., $||P_Dw||_{\widetilde{S}}^2/||w||_{\widetilde{S}}^2 \leq C$ for all $w \in \{w \in \widetilde{W} \,|\, U^TBw = 0\}$ for $C > 0$. An estimate of this type will be established in Lemma 6.1. Then, based on results of [36], it was shown in [32, Lemma 3.2] that the condition number of the FETI-DP operator preconditioned by deflation/projector preconditioning or balancing can be bounded from above by C.

Let us briefly comment on the computational cost. We use deflation or balancing as a second, independent mechanism (in addition to an initial coarse space from partial assembly; see (3.1)) to implement the coarse space constructed from our eigenvalue problems. Other approaches to implement this coarse space would also be possible. For the deflation or balancing approach, the coarse operator U^TFU has to be formed as a sparse matrix and, during the iteration, the application of $(U^TFU)^+$ to a vector has to be computed. When forming the Galerkin product U^TFU, it is essential for the efficiency to exploit the sparsity of U and the structure of F. The pseudoinverse $(U^TFU)^+$ can be computed at essentially the same cost as a sparse Cholesky factorization. However, for large adaptive coarse problems, the computational cost can still be large.

5. Adaptive coarse spaces, geometry issues for irregular partitioning, and enforcing constraints. In the following, we will introduce a modified variant of the 3D algorithm presented in [45], which is based on face eigenvalue problems, extended by some new edge eigenvalue problems of similar pattern. Let us consider the face $\mathcal{F}^{ij}$ between the subdomains Ω_i and Ω_j as well as its closure $\overline{\mathcal{F}}^{ij}$. For the basic algorithm we proceed as in [44] by using the notation from [32] and define $B_{F_{ij}} = [B_{F_{ij}}^{(i)} B_{F_{ij}}^{(j)}]$ as the submatrix of $[B^{(i)}B^{(j)}]$ consisting of all the rows that contain exactly one $+1$ and one -1. Analogously, $B_{D,F_{ij}} = [B_{D,F_{ij}}^{(i)} B_{D,F_{ij}}^{(j)}]$ will be the scaled

submatrix of $[B_D^{(i)} B_D^{(j)}]$. Let us note that the scalings used in the local eigenvalue problems are the localized scalings from the FETI-DP algorithm, i.e., for a node on the edge between three subdomains Ω_i, Ω_j, and Ω_k, the scaling for the jump $w_i - w_j$ in the corresponding eigenvalue problem is $\delta_i^\dagger = \rho_i/(\rho_i + \rho_j + \rho_k)$ if ρ-scaling is used.

We then define

$$S_{ij} := \begin{bmatrix} S^{(i)} & 0 \\ 0 & S^{(j)} \end{bmatrix}, \qquad P_{D_{ij}} := B_{D,F_{ij}}^T B_{F_{ij}}.$$

By $\widetilde{W}_{ij}$ we denote the space of functions in $W_i \times W_j$ that are continuous in the primal variables shared by Ω_i and Ω_j and by Π_{ij} the ℓ_2-orthogonal projection from $W_i \times W_j$ to $\widetilde{W}_{ij}$. We introduce a second ℓ_2-orthogonal projection from $W_i \times W_j$ to range $(\Pi_{ij} S_{ij} \Pi_{ij} + \sigma(I - \Pi_{ij}))$ which is denoted by $\overline{\Pi}_{ij}$, and where σ is a positive constant, e.g., the maximum of the diagonal entries of S_{ij}. We just note that we build both of them so that they are symmetric and we will explain in detail how to obtain Π_{ij} and $\overline{\Pi}_{ij}$ after Remark 1.

We now establish and solve the following generalized eigenvalue problems

$$\overline{\Pi}_{ij} \Pi_{ij} P_{D_{ij}}^T S_{ij} P_{D_{ij}} \Pi_{ij} \overline{\Pi}_{ij} w_{ij}^k = \mu_{ij}^k (\overline{\Pi}_{ij} (\Pi_{ij} S_{ij} \Pi_{ij} + \sigma(I - \Pi_{ij})) \overline{\Pi}_{ij} + \sigma(I - \overline{\Pi}_{ij})) w_{ij}^k, \tag{5.1}$$

for $\mu_{ij}^k \geq$TOL. Thus, for every eigenvalue problem for $w_{ij} \in W_i \times W_j$ we will just consider the jumps $w_i - w_j$ across the closure $\overline{\mathcal{F}}^{ij}$ of the face $\mathcal{F}^{ij}$. We remark that Π_{ij} removes the rigid body modes of each of the single substructures Ω_i and Ω_j while $I - \overline{\Pi}_{ij}$ is an orthogonal projection onto the space of rigid body modes that are continuous on $W_i \times W_j$ and move Ω_i and Ω_j as a connected entity. Consequently, the right hand side of the eigenvalue problem (5.1) is symmetric positive definite; cf. [44].

This eigenvalue problem can be motivated by the localization of the global P_D operator, which is at the center of the condition number proof of FETI-DP and BDDC methods; cf. the penultimate paragraph of Section 4: Define the bilinear form $s_{ij}(\cdot,\cdot) := (\cdot, S_{ij}\cdot)$ for $u_{ij} \times v_{ij}$ with $u_{ij}, v_{ij} \in W_i \times W_j$. The local generalized eigenvalue problem (5.1) can then be given alternatively by the variational formulation: Find $w_{ij}^k \in (\ker S_{ij})^\perp$, such that

$$s_{ij}(P_{D_{ij}} v_{ij}, P_{D_{ij}} w_{ij}^k) = \mu_{ij}^k s_{ij}(v_{ij}, w_{ij}^k) \quad \forall v_{ij} \in (\ker S_{ij})^\perp.$$

A more detailed motivation, based on the local estimate for faces (5.6), can be found in [44, Sections 4 and 5] and [45, Section 3]. Note that essentially the same motivation can be given for our edge eigenvalue problem introduced in (5.4) below.

Note that the eigenvalue problems are defined for closed faces. As already proposed in [45, p.1819], we split the computed face constraint columns $u_{ij}^k := B_{D,F_{ij}} S_{ij} P_{D_{ij}} w_{ij}^k$ into several edge parts $u_{ij,\mathcal{E}_m}^k$ and a part on the open face $u_{ij,\mathcal{F}}^k$, all extended by zero to the closure of the face. We then enforce not only the open face constraint but all the constraints

$$u_{ij,\mathcal{E}_m}^{k\,T} B_{F_{ij}} w_{ij} = 0, \quad m = 1, 2, \ldots, \tag{5.2}$$

$$u_{ij,\mathcal{F}}^{k\,T} B_{F_{ij}} w_{ij} = 0. \tag{5.3}$$

We will refer to the edge constraints in (5.2) as "*edge constraints from face eigenvalue problems*"; see also the numerical experiments in Section 8.

Clearly, since $u_{ij}^k = u_{ij,\mathcal{F}}^k + \sum_m u_{ij,\mathcal{E}_m}^k$, we then also have ${u_{ij}^k}^T B_{F_{ij}} w_{ij} = 0$. With this approach, we avoid coupling of constraints on the closure of the faces which would spoil the block structure of the constraint matrix U; cf. [45]. Thus, from a single eigenvector defined on a closed face, in case of a structured decomposition into cubes, we would obtain one face constraint and 4 edge constraints.

In order to control the jumps $w_i - w_l$ for subdomains Ω_i, Ω_l that only share an edge; compare Figure 5.1, we additionally solve the eigenvalue problems

$$\overline{\Pi}_{il}\Pi_{il}P_{D_{il}}^T S_{il} P_{D_{il}}\Pi_{il}\overline{\Pi}_{il} w_{il}^k = \mu_{il}^k(\overline{\Pi}_{il}(\Pi_{il}S_{il}\Pi_{il} + \sigma(I-\Pi_{il}))\overline{\Pi}_{il} + \sigma(I-\overline{\Pi}_{il}))w_{il}^k \tag{5.4}$$

for $\mu_{il}^k \geq$TOL and with Π_{il} and $\overline{\Pi}_{il}$ constructed in the same manner as Π_{ij} and $\overline{\Pi}_{ij}$ before.

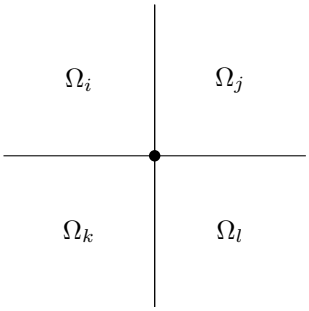

Figure 5.1: Cross section view of four subdomains sharing an edge in a regular partition; Ω_i shares faces with Ω_j and Ω_k but only an edge with Ω_l.

Clearly, this only has to be carried out for edges shared by more than three subdomains and also in some cases where the open face does not contain any nodes. We refer to [52] where experiments showed that typically around 99% of the edges are common to exactly three subdomains when an automatic graph partitioner is used. Hence, for automatically partitioned domains, which we consider as the standard case, these new eigenvalue problems just come into play for either a small number of edges or a slightly larger number of small edges. Therefore, the extra work for solving the edge eigenvalue problems is small. We will come back to this matter and discuss the cost and necessity of edge eigenvalue problems in practice in Section 8.

Finally, the constraints resulting from edge eigenvalue problems are

$${w_{il}^k}^T P_{D_{il}}^T S_{il} P_{D_{il}} w_{il} = 0. \tag{5.5}$$

As in the two-dimensional case (see [33]), locally, for $w_{ij} \in W_i \times W_j$, $w_{il} \in W_i \times W_l$ which satisfy the constraints, the estimates

$$w_{ij}^T \overline{\Pi}_{ij}\Pi_{ij}P_{D_{ij}}^T S_{ij} P_{D_{ij}}\Pi_{ij}\overline{\Pi}_{ij} w_{ij} \leq \text{TOL}\, w_{ij}^T \overline{\Pi}_{ij}\Pi_{ij} S_{ij}\Pi_{ij}\overline{\Pi}_{ij} w_{ij}, \tag{5.6}$$

$$w_{il}^T \overline{\Pi}_{il}\Pi_{il}P_{D_{il}}^T S_{il} P_{D_{il}}\Pi_{il}\overline{\Pi}_{il} w_{il} \leq \text{TOL}\, w_{il}^T \overline{\Pi}_{il}\Pi_{il} S_{il}\Pi_{il}\overline{\Pi}_{il} w_{il} \tag{5.7}$$

hold. With [3, Section 2.7], this can be derived from the fact that Π_{ij} and $\overline{\Pi}_{ij}$ commute and the fact that $\Pi_{is}(I - \overline{\Pi}_{is})w_{is} = (I - \overline{\Pi}_{is})w_{is}$. The last feature is obtained since $(I - \overline{\Pi}_{is})$ is an orthogonal projection onto the space of rigid body modes that are continuous on $W_i \times W_s$. Note that the same arguments can be used for edge eigenvalue problems, too. Obviously, (5.7) does only apply to subdomains Ω_i having edges $\mathcal{E}$ shared by subdomains Ω_l without a common face $\mathcal{F}^{il}$.

We will now use the index $s \in \{j, l\}$ to describe simultaneously face ($s = j$) and edge ($s = l$) eigenvalue problems and their operators.

We still have to show that the local estimates from above, for functions fulfilling the constraints, are also valid for all $w_{is} \in W_i \times W_s$ derived from a restriction of $w \in \widetilde{W}$ to $W_i \times W_s$, since this will be used in the FETI-DP condition number proof.

Hence, for $s = j$ or $s = l$ let Π_{is} be as above. Then, for $w \in \widetilde{W}$ we have

$$\begin{bmatrix} R^{(i)}w \\ R^{(s)}w \end{bmatrix} \in \widetilde{W}_{is}, \quad \text{and therefore} \quad \Pi_{is} \begin{bmatrix} R^{(i)}w \\ R^{(s)}w \end{bmatrix} = \begin{bmatrix} R^{(i)}w \\ R^{(s)}w \end{bmatrix}. \tag{5.8}$$

Exactly as in [32], we argue as follows. $\Pi_{is}(I - \overline{\Pi}_{is})w_{is} = (I - \overline{\Pi}_{is})w_{is}$ yields $P_{D_{is}}\Pi_{is}(I - \overline{\Pi}_{is})w_{is} = 0$ and $S_{is}\Pi_{is}(I - \overline{\Pi}_{is})w_{is} = 0$. Since we can split any w_{is}^k resulting from the local eigenvalue problem (5.1) or (5.4) as $w_{is}^k = (I - \overline{\Pi}_{is})w_{is}^k + \overline{\Pi}_{is}w_{is}^k$ it therefore holds

$$w_{is}^T \Pi_{is} P_{D_{is}}^T S_{is} P_{D_{is}} \Pi_{is} w_{is} \leq \text{TOL} w_{is}^T \Pi_{is} S_{is} \Pi_{is} w_{is} \tag{5.9}$$

for all w_{is} in $W_i \times W_s$ with ${w_{is}^k}^T P_{D_{is}}^T S_{is} P_{D_{is}} w_{is} = 0$, $\mu_{is}^k \geq \text{TOL}$. Therefore, the estimate is valid for $w_{is} \in \widetilde{W}_{is}$ which satisfies the constraints; cf. [44].

REMARK 1. *In order to guarantee that* TOL *is finite for all $w_{is} \in \widetilde{W}_{is}$ we have to treat the kernel of S_{is} correctly. As already mentioned by [44, Assumption 8] or [55, Assumption 29] we have to ensure,*

$$\forall w_{is} \in \widetilde{W}_{is} : S_{is}w_{is} = 0 \Rightarrow B_{is}w_{is} = 0. \tag{5.10}$$

Thus, we have to be aware of $\dim(\Pi_{is} \ker S_{is}\Pi_{is}) = 7$ *if* $\ker S_{is} = 12$ *(or comparably if at least one subdomain has Dirichlet boundary conditions). This can result from an additional hinge mode, i.e., a rigid body rotation of the two subdomains around the common edge. In order to ensure the assumption* (5.10) *we select at least two primal vertices on straight edges. For nonstraight or bent edges we will have to select a third primal vertex that is not located on the straight line between the other two vertices on the edge; to prevent the hinge mode that would violate* (5.10)*. We remark that the existence of sufficient vertices on an edge is, in general, not ensured if we use a graph partitioner and a common understanding of edges and vertices; see, e.g., [38, Def. 3.1]. We thus transform arbitrary dual nodes that fulfill the given restrictions into primal vertices.*

Completely analogously to [51], we build Π_{is} and $\overline{\Pi}_{is}$. By defining $R_{is}^{(k)T}$, $k = i, s$ as the assembly operator of primal variables on $\partial\Omega_i \cap \partial\Omega_s$ and identity on the rest of $\Gamma^{(i)} \times \Gamma^{(s)}$, we obtain

$$R_{is} := \begin{pmatrix} R_{is}^{(i)} \\ R_{is}^{(s)} \end{pmatrix}$$

and the orthogonal projection onto $\widetilde{W}_{is}$,

$$\Pi_{is} := R_{is}(R_{is}^T R_{is})^{-1} R_{is}^T.$$

We note that the inverse can be computed cheaply since R_{is} contains a large identity block and a very small block of the size of the number of the degrees of freedom that are common to the two subdomains. For the construction of $\overline{\Pi}_{is}$ we exploit the fact that $I - \overline{\Pi}_{is}$ is an orthogonal projection onto the rigid body modes that are continuous on $W_i \times W_s$. For straight edges and subdomains only connected by this edge and without sufficient Dirichlet boundary the hinge mode mentioned before is in fact a rigid body mode and will be used to establish the projection $\overline{\Pi}_{il}$. If $\{\tilde{r}_1, \ldots, \tilde{r}_k\}$ is the set of rigid body modes that are continuous on $W_i \times W_s$ we use a modified Gram-Schmidt method to create an orthonormal basis $\{r_1, \ldots, r_k\}$ and define $\overline{\Pi}_{is} = I - \sum_{i=1}^k r_i r_i^T$. The adaptively computed constraints coming from eigenvalue problems will then be enforced by a deflation approach; in all simulations we exclusively use the balancing preconditioner.

6. Condition number estimate. Before we are able to provide the theoretical bound on the condition number of the preconditioned FETI-DP operator we have to present an analytical expression for the application of the localized P_D-operator; cf. the definition of the P_D-operator at the end of Section 4.

The local operators $P_{D_{ij}}$ and $P_{D_{il}}$ on the closure of the face and edge, respectively, are

$$P_{D_{ij}} = \begin{bmatrix} B_{D,F_{ij}}^{(i)T} B_{F_{ij}}^{(i)} & B_{D,F_{ij}}^{(i)T} B_{F_{ij}}^{(j)} \\ B_{D,F_{ij}}^{(j)T} B_{F_{ij}}^{(i)} & B_{D,F_{ij}}^{(j)T} B_{F_{ij}}^{(j)} \end{bmatrix} \text{ and } P_{D_{il}} = \begin{bmatrix} B_{D,E_{il}}^{(i)T} B_{E_{il}}^{(i)} & B_{D,E_{il}}^{(i)T} B_{E_{il}}^{(l)} \\ B_{D,E_{il}}^{(l)T} B_{E_{il}}^{(i)} & B_{D,E_{il}}^{(l)T} B_{E_{il}}^{(l)} \end{bmatrix};$$

see [32]. For a face $\mathcal{F}^{ij}$ with edges $\mathcal{E}_1^{ij}, \ldots, \mathcal{E}_m^{ij}$, $m \geq 3$, we define the cutoff function on the closure of the face

$$\vartheta_{\mathcal{F}^{ij}} := \theta_{\mathcal{F}^{ij}} + \sum_{p=1}^{m} \theta_{\mathcal{E}_p^{ij}}. \tag{6.1}$$

We can use the cutoff function $\theta_{\mathcal{E}_p^{ij}}$ on the open edge since all vertices were chosen to be primal. For $w \in \widetilde{W}$, this gives

$$P_{D_{ij}} \begin{bmatrix} R^{(i)} w \\ R^{(j)} w \end{bmatrix} = \begin{bmatrix} I^h(\vartheta_{\mathcal{F}^{ij}} D_j(w_i - w_j)) \\ I^h(\vartheta_{\mathcal{F}^{ij}} D_i(w_j - w_i)) \end{bmatrix}, \tag{6.2}$$

where I^h is the finite element interpolation operator on Ω_i and Ω_j, respectively. For the sake of simplicity, we assume that just $\mathcal{E}_1^{ij} = \mathcal{E}^{il}$ has a multiplicity greater than three and equal to four with $w_i - w_l$ as the problematic jump between two subdomains sharing at least one edge but no face; see Figure 5.1. Other cases can be handled in the same way. The application of the local P_D-operator of the edge eigenvalue problem yields

$$P_{D_{il}} \begin{bmatrix} R^{(i)} w \\ R^{(l)} w \end{bmatrix} = \begin{bmatrix} I^h(\theta_{\mathcal{E}^{il}} D_l(w_i - w_l)) \\ I^h(\theta_{\mathcal{E}^{il}} D_i(w_l - w_i)) \end{bmatrix}. \tag{6.3}$$

Let $U = (u_1, \ldots, u_k)$ be given as the matrix where the adaptively computed constraints are stored as columns , i.e., the constraints defined in (5.2), (5.3), and (5.5) extended by zero to the space of all Lagrange multipliers to fit the dimension. By $\widetilde{W}_U := \{w \in \widetilde{W} \,|\, U^T B w = 0\}$ we denote the subspace of $\widetilde{W}$ which contains those elements $w \in \widetilde{W}$ satisfying the new constraints, i.e., $Bw \in \ker U^T$.

LEMMA 6.1. *Let $N_{\mathcal{F}}$ denote the maximum number of faces of a subdomain, $N_{\mathcal{E}}$ the maximum number of edges of a subdomain, $M_{\mathcal{E}}$ the maximum multiplicity of an edge and* TOL *a given tolerance for solving the local generalized eigenvalue problems. We assume that all vertices are chosen to be primal. Then, for $w \in \widetilde{W}_U$, we have*

$$|P_D w|_{\widetilde{S}}^2 \leq 4 \max\{N_{\mathcal{F}}, N_{\mathcal{E}} M_{\mathcal{E}}\}^2 \text{TOL} |w|_{\widetilde{S}}^2.$$

Proof. We first have a closer look at the global operator P_D and its restriction to a subdomain. Since all vertices are primal, we obtain

$$v_i := R^{(i)} P_D w = \sum_{\mathcal{F}^{ij} \subset \partial\Omega_i} I^h(\theta_{\mathcal{F}^{ij}} v_i) + \sum_{\mathcal{E}^{il} \subset \partial\Omega_i} I^h(\theta_{\mathcal{E}^{il}} v_i); \tag{6.4}$$

see, e.g., [62, Sec. 6.4.3].

In contrast to other proofs on the condition number of the FETI-DP system, where the additive terms of (6.4) are bounded separately, we will now rearrange these additive terms. This is due to the fact that the face eigenvalue problems are solved on the closure of the faces.

Therefore, we introduce a global and N local sets of pairs of indices $\{i,l\}$, where each index pair represents an edge eigenvalue problem on $\mathcal{E}^{il}$ and vice versa, i.e.,

$$\begin{aligned}\mathcal{E}^* := \{\{j,l\} : 1 \le j,l \le N,\, \mu_1(\partial\Omega_j \cap \partial\Omega_l) > 0,\, \mu_2(\partial\Omega_j \cap \partial\Omega_l) = 0\}\\ \text{and, for } i = 1,\dots,N, \quad \mathcal{E}_i^* := \{\{j,l\} \subset \mathcal{E}^* : j = i \vee l = i\}.\end{aligned}$$

Here, μ_d is the d-dimensional Lebesgue measure. Thus, $\{j,l\} \in \mathcal{E}^*$ means that the subdomains Ω_j and Ω_l share at least an edge but no face. In general, for subdomains obtained from graph partitioners, these sets do not contain many elements as already mentioned before.

For a given face $\mathcal{F}^{ij}$, we now denote the edges which are part of the closure of the face by $\mathcal{E}_1^{ij},\dots,\mathcal{E}_m^{ij}$. In order to avoid the proliferation of indices we take an arbitrary edge $\mathcal{E}^{ij} \in \{\mathcal{E}_1^{ij},\dots,\mathcal{E}_m^{ij}\}$ that is shared by Ω_i and $\Omega_{r_1},\dots,\Omega_{r_p}$ with $r_1,\dots,r_p \in \{1,\dots,N\} \setminus \{i\}$. We then have the interpolation operators

$$I^h(\theta_{\mathcal{F}^{ij}} v_i) = I^h(\theta_{\mathcal{F}^{ij}} D_j(w_i - w_j)), \tag{6.5}$$

$$I^h(\theta_{\mathcal{E}^{ij}} v_i) = I^h(\theta_{\mathcal{E}^{ij}}(D_{r_1}(w_i - w_{r_1}) + \ldots + D_{r_p}(w_i - w_{r_p})). \tag{6.6}$$

Obviously, for each edge $\mathcal{E}^{ij} \in \{\mathcal{E}_1^{ij},\dots,\mathcal{E}_m^{ij}\}$ the term $I^h(\theta_{\mathcal{E}^{ij}}(D_j(w_i - w_j))$ is part of (6.6). For each edge $\mathcal{E}^{ij}$, we subtract it from (6.6) and add it to (6.5). The remaining jumps in (6.6) can then either be added analogously to the corresponding face term

$$I^h(\theta_{\mathcal{F}^{irs}} D_{r_s}(w_i - w_{r_s}))$$

(cf. (6.5)), if such a face exists, or they remain in (6.6).

If this is carried out for all faces and edges analogously (6.4) becomes

$$R^{(i)} P_D w = \sum_{\mathcal{F}^{ij} \subset \partial\Omega_i} I^h(\vartheta_{\mathcal{F}^{ij}} D_j(w_i - w_j)) + \sum_{\{i,l\} \in \mathcal{E}_i^*} I^h(\vartheta_{\mathcal{E}^{il}} D_l(w_i - w_l)). \tag{6.7}$$

Here, we have replaced the cutoff functions for the open edges by those for the closure of these edges, that is $\vartheta_{\mathcal{E}} = 1$ at the endpoints of the edge and $\vartheta_{\mathcal{E}} = \theta_{\mathcal{E}}$ for all other nodes of the mesh. This can be done since all vertices are primal. We define the S_k-seminorm $|\cdot|_{S_k} := \langle \cdot, S^{(k)} \cdot \rangle$ for $k = i, j$.

Then, we estimate the face terms in (6.7) similar to the edge terms in 2D; see [32]. The remaining edge terms in (6.7) can be estimated by using the constraints obtained from the edge eigenvalue problems.

For $w \in \widetilde{W}_U$, $w_k = R^{(k)} w$, $k \in \{i,j,l\}$, we have

$$\begin{aligned}|P_D w|_S^2 &= \sum_{i=1}^N |R^{(i)} P_D w|_{S_i}^2\\ &\overset{(6.7)}{\le} 2\max\{N_{\mathcal{F}}, N_{\mathcal{E}} M_{\mathcal{E}}\} \sum_{i=1}^N \left[\sum_{\mathcal{F}^{ij} \subset \partial\Omega_i} |I^h(\vartheta_{\mathcal{F}^{ij}} D_j(w_i - w_j))|_{S_i}^2 \right.\end{aligned}$$

$$
\begin{aligned}
&\quad + \sum_{\{i,l\}\in\mathcal{E}_i^*} |I^h(\vartheta_{\mathcal{E}^{il}} D_l(w_i - w_l))|^2_{S_i} \Bigg] \\
&= 2\max\{N_{\mathcal{F}}, N_{\mathcal{E}} M_{\mathcal{E}}\} \Bigg[\sum_{\mathcal{F}^{ij}\subset\Gamma} \left[|I^h(\vartheta_{\mathcal{F}^{ij}} D_j(w_i - w_j))|^2_{S_i} + |I^h(\vartheta_{\mathcal{F}^{ij}} D_i(w_j - w_i))|^2_{S_j} \right] \\
&\quad + \sum_{\{i,l\}\in\mathcal{E}^*} \left[|I^h(\vartheta_{\mathcal{E}^{il}} D_l(w_i - w_l))|^2_{S_i} + |I^h(\vartheta_{\mathcal{E}^{il}} D_i(w_l - w_i))|^2_{S_l} \right] \Bigg] \\
&\overset{(6.2),(6.3),(5.8)}{=} 2\max\{N_{\mathcal{F}}, N_{\mathcal{E}} M_{\mathcal{E}}\} \Bigg[\sum_{\mathcal{F}^{ij}\subset\Gamma} \begin{bmatrix} w_i \\ w_j \end{bmatrix}^T \Pi_{ij} P_{D_{ij}}^T \begin{bmatrix} S^{(i)} & 0 \\ 0 & S^{(j)} \end{bmatrix} P_{D_{ij}} \Pi_{ij} \begin{bmatrix} w_i \\ w_j \end{bmatrix} \\
&\quad + \sum_{\{i,l\}\in\mathcal{E}^*} \begin{bmatrix} w_i \\ w_l \end{bmatrix}^T \Pi_{il} P_{D_{il}}^T \begin{bmatrix} S^{(i)} & 0 \\ 0 & S^{(l)} \end{bmatrix} P_{D_{il}} \Pi_{il} \begin{bmatrix} w_i \\ w_l \end{bmatrix} \Bigg] \\
&\overset{(5.9)}{\leq} 2\max\{N_{\mathcal{F}}, N_{\mathcal{E}} M_{\mathcal{E}}\}\mathrm{TOL} \Bigg[\sum_{\mathcal{F}^{ij}\subset\Gamma} \begin{bmatrix} w_i \\ w_j \end{bmatrix}^T \Pi_{ij} \begin{bmatrix} S^{(i)} & 0 \\ 0 & S^{(j)} \end{bmatrix} \Pi_{ij} \begin{bmatrix} w_i \\ w_j \end{bmatrix} \\
&\quad + \sum_{\{i,l\}\in\mathcal{E}^*} \begin{bmatrix} w_i \\ w_l \end{bmatrix}^T \Pi_{il} \begin{bmatrix} S^{(i)} & 0 \\ 0 & S^{(l)} \end{bmatrix} \Pi_{il} \begin{bmatrix} w_i \\ w_l \end{bmatrix} \Bigg] \\
&\overset{(5.8)}{=} 2\max\{N_{\mathcal{F}}, N_{\mathcal{E}} M_{\mathcal{E}}\}\mathrm{TOL} \Bigg[\sum_{\mathcal{F}^{ij}\subset\Gamma} \left[|w_i|^2_{S_i} + |w_j|^2_{S_j} \right] + \sum_{\{i,l\}\in\mathcal{E}^*} \left[|w_i|^2_{S_i} + |w_l|^2_{S_l} \right] \Bigg] \\
&\leq 2\max\{N_{\mathcal{F}}, N_{\mathcal{E}} M_{\mathcal{E}}\}\mathrm{TOL} \left[2\max\{N_{\mathcal{F}}, N_{\mathcal{E}} M_{\mathcal{E}}\} \sum_{i=1}^N |R^{(i)} w|^2_{S_i} \right] \\
&= 4\max\{N_{\mathcal{F}}, N_{\mathcal{E}} M_{\mathcal{E}}\}^2 \mathrm{TOL} |w|^2_{\widetilde{S}}.
\end{aligned}
$$

□

In the next theorem, we provide a condition number estimate for the preconditioned FETI-DP algorithm with all vertex constraints being primal and additional, adaptively chosen edge and face constraints.

THEOREM 6.2. *Let $N_{\mathcal{F}}$ denote the maximum number of faces of a subdomain, $N_{\mathcal{E}}$ the maximum number of edges of a subdomain, $M_{\mathcal{E}}$ the maximum multiplicity of an edge and* TOL *a given tolerance for solving the local generalized eigenvalue problems. If all vertices are chosen to be primal, the condition number $\kappa(\widehat{M}^{-1}F)$ of the FETI-DP algorithm with adaptive constraints as described, e.g., enforced by the deflation preconditioner $\widehat{M}^{-1} = M_{PP}^{-1}$ or the balancing preconditioner $\widehat{M}^{-1} = M_{BP}^{-1}$, satisfies*

$$\kappa(\widehat{M}^{-1}F) \leq 4\max\{N_{\mathcal{F}}, N_{\mathcal{E}} M_{\mathcal{E}}\}^2 \mathrm{TOL}.$$

Proof. The condition number bound for the deflation preconditioner can be given with Lemma 6.1 and [32, Lemma 3.2]. The relation between the eigenvalues of $M_{PP}^{-1}F$ and $M_{BP}^{-1}F$ can be found in [46], or, in our notation in [36]. □

Let us finally note that the constant in the condition number estimate provided by Theorem 6.2 is quite conservative. The geometrical quantities $N_{\mathcal{F}}$, $N_{\mathcal{E}}$, and $M_{\mathcal{E}}$ enter our estimate when the Cauchy-Schwarz inequality is used to estimate the product of

functions supported on faces and edges. These functions are not S_i-orthogonal to each other, but, in practice, their mutual S_i-inner product is small. This is not exclusive to our approach since these quantities already appear implicitly, in a generic constant C, in the traditional (nonadaptive) FETI-DP and BDDC condition number estimates; see, e.g., [43, 38, 62]. It can be observed numerically that often (5.9) provides a more realistic indicator for the condition number, i.e., our results in Section 8 show that the condition number is at the order of TOL in our numerical experiments rather than at the order of $4\max\{N_{\mathcal{F}}, N_{\mathcal{E}}M_{\mathcal{E}}\}^2$TOL. This has already been observed by [44, 45], and the use of (5.9) (for faces) has been proposed as a condition number indicator; see also [55, 56, 57].

7. Reducing the number of eigenvalue problems. In this section, we briefly describe strategies which can help to keep the number of eigenvalue problems as well as the size of the coarse problem small – while still obtaining an acceptable condition number. The first two ideas aim at reducing the number of edge eigenvalue problems; see Section 7.1. The second approach aims at reducing the number of edge constraints; see Section 7.2. The third reduction approach, first suggested in [31], is based on considering the preconditioned starting residual to detect critical edges; see Section 7.3. This strategy was proposed but not implemented in [31].

7.1. Reducing the number of edge eigenvalue problems.

7.1.1. Short edges. In order to reduce the number of edge eigenvalue problems while keeping the theoretical condition number bound, we eliminate all eigenvalue problems related to short edges. There, we set all edge nodes belonging to edge eigenvalue problems as primal if there are not more than k dual nodes on the edge. Throughout this paper, we consider edges as short if they consist of only a single node, i.e., in our experiments, we use $k = 1$. Note that in unstructured decompositions, e.g., from METIS, most edges have a multiplicity of only three. As a result, edge eigenvalue problem are necessary only for a small number of edges and this strategy applies only to the short edges among these. This strategy is always used in our numerical experiments.

7.1.2. Edges at a distance from heterogeneities. Additionally, for compressible elasticity, if no coefficient jumps occur in the neighborhood of an edge, we do not take the corresponding eigenvalue problems into consideration. This is related to slab techniques; see, e.g., [18, 17, 32]. If the coefficient distribution is not available then the diagonal entries of the stiffness matrix can be considered instead. Let us note that, after reducing the number of edge eigenvalue problems, our explicit condition number bound of Theorem 6.2 might not hold anymore in this form. Nevertheless, based on the theory of slab techniques, the condition number is expected to stay bounded independently of the coefficient jumps. This will be confirmed by our numerical experiments in Section 8. The strategy can be implemented by traversing the nodes on the edge while evaluating the coefficient function. If no large heterogeneities are encountered then the edge eigenvalue problem can be discarded. If the coefficient function is not available the diagonal entries of the stiffness matrix can be used, instead. In presence of coefficient jumps combined with almost incompressible components this technique is not advisable since constraints enforcing the essential zero net flux condition may be removed from the coarse space. The number of coefficient jumps encountered while traversing the edge can also be used to define the number of eigenvectors to be used for the edge, i.e., as an alternative to defining a tolerance TOL: If a single heterogeneity is encountered, e.g., a single channel with

a high coefficient crosses the edge, then only one eigenvector will be added to the coarse problem. This corresponds to using a single weighted edge average as first suggested in [35]. Of course, for a larger number of channels more eigenvectors have to be used. In the classical approach [35], it is then necessary to split the weighted edge average [35] into several weighted averages, defined on subsets of the edge, or to introduce additional primal vertex constraints.

7.2. Reducing the number of edge constraints from face eigenvalue problems. The same idea as in Section 7.1.2 can be used to discard certain edge constraints from face eigenvalue problems in order to reduce the size of the coarse problem: Edge constraints from face eigenvalue problems are not added to the coarse space if no coefficient jump is detected in the neighborhood of the edge.

7.3. Heuristics to reduce the number of eigenvalue problems based on the residual. We follow an idea of [31] and assume that the residuals on faces and edges without any jumps are several magnitudes smaller than those on faces and edges with jumps along or across the interface. Therefore, for the closure of any face or edge, generically denoted by Λ, with n Lagrange multipliers we compute $r := M_D^{-1}(d - F\lambda)$ and restrict the preconditioned residual to the closure of the face or edge, that is $r_\Lambda = r_{|\Lambda}$.

Then, we compute $r_{\Lambda,2} := 1/\sqrt{n}\|r_\Lambda\|_2$ to check its magnitude. Another reasonable approach would be to compute the maximum norm of r_Λ, i.e., $r_{\Lambda,\infty}$. In our experiments, we take a combination of these two and check simultaneously for every face or edge if $r_{\Lambda,n} < \tau_2$ and $r_{\Lambda,\infty} < \tau_\infty$. If this is the case we do not consider the corresponding eigenvalue problem and discard it (with all possible constraints). Otherwise we continue as before and compute the constraints from our eigenvalue problems. If the energy norm is used this approach is remotely related to the computation of Rayleigh quotients in [58].

Note that this approach can significantly reduce the number of eigenvalue problems but often results in a coarse space of comparable size. But due to the smaller number of eigenvalue computations, the heuristic approach presented here is computationally less expensive.

8. Numerical results. In this section, we show numerical results for linear elasticity using FETI-DP with the adaptive coarse space strategies discussed before. We compare the coarse spaces introduced in [44, 45] and our new coarse space with edge constraints from edge eigenvalue problems presented in Section 5. We recall that by "edge constraints from face eigenvalue problems" we refer to edge constraints which result from splitting constraints originating from eigenvectors computed on the (closed) face; see (5.2) in Section 5.

We have implemented the new coarse space covered by our theory, see Lemma 6.2, and two modifications thereof. In our tables, the three approaches will be denoted by 'Algorithms Ia, Ib, and Ic'. '*Algorithm Ia*' is the algorithm covered by our theory. It will make use of the largest number of eigenvalue problems and will lead to the most generous coarse problem. '*Algorithm Ib*' uses the neighborhood approach of Section 7.1.2 to reduce the number of edge eigenvalue problems if they are not needed. '*Algorithm Ic*' makes use of the neighborhood approach described in Section 7.2, in addition to the reduction approach of Section 7.1.2, to reduce the size of the coarse space by discarding edge constraints from face eigenvalue problems which are not needed.

Furthermore, we will test two variants of the classical approach of [44, 45]. These

approaches do not use edge eigenvalue problems. As '*Algorithm II*', we will denote the coarse space proposed in [44, 45], where all edge constraints from face eigenvalue problems are enforced as additional constraints. To the best of our knowledge, this approach has not been implemented and tested before; cf. [55, 56, 45, 57]. As '*Algorithm III*' we will denote the "classic" adaptive approach already tested extensively in [44, 45]. In this approach, all edge constraints from face eigenvalue problems are simply discarded, which results in a smaller coarse problem at the cost of losing robustness.

We use balancing to implement all adaptive constraints; cf. Section 4. For all algorithms, the columns of U are orthogonalized blockwise (i.e., edge- and facewise) by a singular value decomposition with a drop tolerance of $1e-6$. Let us note, again, that our current theory from Lemma 6.2 covers Algorithm Ia. Although Algorithm Ib and Ic are both not covered by the theory lined out in this paper, we will show that in our experiments they will give almost the same results as Algorithm Ia. Algorithm II and III are not covered by the theory, and our numerical results will indeed show that they cannot guarantee low condition numbers and iterations counts for all our test cases.

In all cases of either compressible or incompressible linear elasticity the edge eigenvalue reduction strategy from Section 7.1.1 is used. Since the strategies used in Algorithm Ib and Ic are based on Young's modulus E, and not Poisson's ratio ν, we will not use the strategies for our test problems of almost incompressible elasticity. For these problems, we will only report on Algorithm Ia.

For simplicity, we always assume the parameters E and ν to be constant on each fine element. As scaling we use ρ-scaling in form of patch-ρ-scaling, and we set Young's modulus at a node by the maximum of all values over the support of the corresponding nodal basis function; cf. [35].

In the experiments, regular as well as irregular decompositions are tested. The irregular decomposition is performed by the METIS graph partitioner [23] using the options `-ncommon=3` for compressible, `-ncommon=4` for incompressible elasticity and `-contig` to avoid noncontiguous subdomains as well as additional hinge modes inside single subdomains.

In all tables, "κ" denotes the condition number of the preconditioned FETI-DP operator, "its" is the number of iterations of the pcg algorithm and "$|U|$" denotes the size of the corresponding second coarse space implemented by deflation or balancing; see Section 4. By N we denote the number of subdomains. For regular as well as irregular decompositions, we define $H = 1/\sqrt[3]{N}$ and thus can define H/h also in the irregular case. For our modified coarse space, we also give the number of edge eigenvalue problem as "$\#\mathcal{E}_{evp}$" and in parentheses the percentage of these in the total number of eigenvalue problems. Our stopping criterion for the pcg algorithm is a relative reduction of the starting residual by 10^{-10}, and the maximum number of iterations is set to 500. The condition numbers κ, which we report in the tables, are estimates from the Krylov process. In our tables, we will mark (estimated) condition numbers below 50 in bold face to indicate that a sufficently large coarse space has been found by the adaptive method. If not stated otherwise, the eigenvalue problems are solved by the MATLAB "eig" function.

For the numerical experiments presented in this paper, we use TOL = 10. The resulting condition number is then typically at the order of TOL; cf. the remark at the end of Section 6 on the use of (5.9) as a condition number indicator; see also the numerical results later in this section. Note that, although our algorithm is algebraic

and thus appears to be black-box, the efficiency of the method relies on properties of the underlying PDE. Therefore, in practice, TOL should be adapted to H/h, i.e., to the classical condition number bound $\kappa \leq C(1 + \log(H/h)^2$. Otherwise, for growing H/h, the coarse problem can become large. For a small tolerance, the adaptive FETI-DP method can even degenerate to a direct solver.

It is clear that Algorithms Ia, Ib, and II will result in a larger coarse space than Algorithm III or Algorithm Ic. For simple test examples, Algorithm Ic should reduce to Algorithm III. Our numerical results will show that, in certain difficult cases, the larger coarse space is indeed necessary.

We will give a short overview on the next subsections.

1. Section 8.1: **Composite materials**. In this section, we will consider composite materials with regular and irregular decompositions into subdomains. We will show that the classic algorithm of [44, 45] is sufficient when there are no coefficient jumps at subdomain edges (see the examples with regular decompositions) but that our extended coarse space (see Sections 5 and 6) is often indispensable when irregular decompositions are used.
2. Section 8.2: **Steel microstructure**. In this section, we will a consider a representative volume element (RVE) of a modern steel and again consider regular and irregular decompositions into subdomains.
3. Section 8.3: **Randomized coefficient distributions**. In this section, we will consider random coefficient distributions combined with irregular decompositions into subdomains. We will vary the volume fraction of the stiff material and consider 100 random coefficient distributions. We will again see that our coarse space is indispensable, here.
4. Section 8.4: **Almost Incompressible Linear Elasticity**. In this section, we will consider different sample materials with almost incompressible components using irregular decompositions into subdomains. Here, for some examples, the classic approach is sufficient but other examples require our enriched coarse space.
5. Section 8.5: **Heuristic approach on reducing the number of eigenvalue problems and constraints based on the residual**. In this section, we will consider examples from the previous sections, combined with the heuristic approach of Section 7.3. We show that our strategy can work well although Theorem 6.1 is not valid anymore.
6. Section 8.6: **Efficiently solving the eigenvalue problems**. In this section, we will briefly consider the cost of building and solving the eigenvalue problems exactly and use favorable approximate solvers to show that approximate solutions of the eigenvectors also give low condition numbers and iteration counts.

8.1. Composite materials.

Regular partitioning. We consider a linear elastic and compressible material on a unit cube, see Figures 8.1 and 8.2, using a structured fine mesh consisting of cubes each decomposed into five tetrahedral finite elements. We enforce zero Dirichlet boundary conditions on the face with $x = 0$ and have zero Neumann boundary conditions elsewhere. We apply a volume force $f := [0.1, 0.1, 0.1]^T$.

First, we use $\nu = 0.3$ for the complete computational domain, and we test different distributions of Young's modulus E. Our first examples are two different (model) composite materials consisting of a soft matrix material with $\mathrm{E}_1 = 1$ and stiff inclusions with $\mathrm{E}_2 = 1e + 06$. The stiff inclusions in the form of beams, arranged in a

regular pattern, span from the face with $x = 0$ straight to the face with $x = 1$. In the first composite material, there are $N^{2/3}$ many beams. In a regular decomposition into cubes we have one centered beam per subdomain, precisely; see Figure 8.1. The intersection of the beams with the face $x = 0$ represents 1/9th of the area of the face. The second composite materials consists of $4N^{2/3}$ many beams as depicted in Figure 8.2. The intersection of the beams with the face $x = 0$ here represents 4/25th of the area of the face.

If a regular decomposition is used with these coefficient configurations, already the classic approach from [44] performs well. We therefore only briefly present the composite material no. 2 in Table 8.1. We see that for this simple case, where the jumps do not cut through edges, all approaches lead to low condition numbers and a low number of iterations. The most simple algorithm, i.e., Algorithm III performs well while resulting in the smallest coarse space. Algorithm Ic automatically reduces to Algoritm III, and therefore gives the same performance. This illustrates the effectiveness of the neighborhood strategies from Section 7.1.2 and 7.2. For this problem, the use of edge constraints can reduce the number of iterations further but not significantly. This shows that edge constraints from face eigenvalue problems (Algorithm II) are not needed, here. The same is true for edge eigenvalue problems (Algorithm Ia).

In structured decompositions, we have a high number of edge eigenvalue problems in Algorithm Ia, i.e., around 50%; if the strategy to reduce the number of edge eigenvalue problems from Section 7.1.2 is applied, all edge eigenvalue problems are discarded while the results remain good; cf. Algorithm Ib and column 6 "$\mathcal{E}_{evp}$" in Table 8.1. This is possible in this simple setting where there are no cuts of coefficient jumps through edges. Note that we do not reduce the coarse problem size; see Table 8.1. In addition, we see that Algorithm Ic reduces to Algorithm III in these cases.

REMARK 2. *We always use the strategy described in Section 7.1.1, i.e., on short edges we never compute edge eigenvalue problems but rather set the corresponding edge nodes as primal. This means that our initial coarse space for all algorithms, i.e., Algorithm I, II, and III, is richer than the standard vertex coarse space.*

Irregular partitioning. In a next step, we consider an irregular decomposition; see Tables 8.2 and 8.3 for composite material no. 1 ($H/h = 3$ and $H/h = 6$) and Tables 8.4 and 8.5 for composite material no. 2 ($H/h = 5$ and $H/h = 10$).

In this case, jumps along and across subdomain edges are very likely to occur.

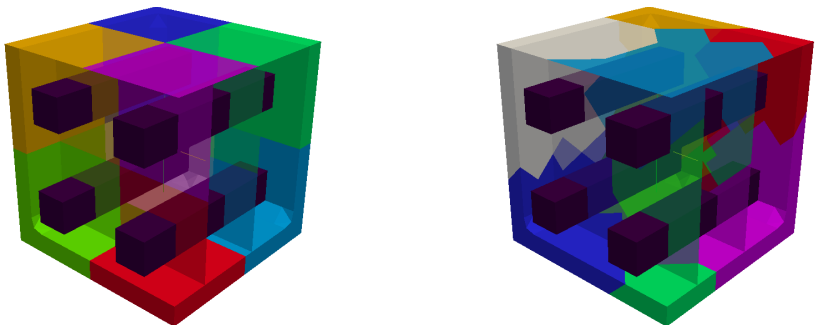

Figure 8.1: Composite material no. 1 using a regular (left) and an irregular (right) decomposition. High coefficients $\mathrm{E}_2 = 1e{+}06$ are shown in dark purple in the picture, subdomains shown in different colors in the background and by half-transparent slices. Visualization for $N = 8$ and $H/h = 3$.

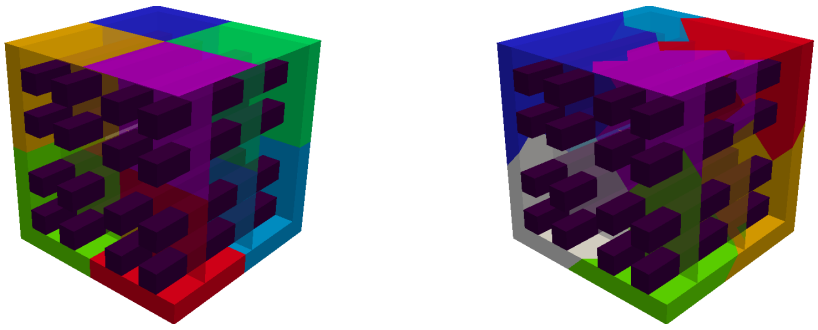

Figure 8.2: Composite material no. 2 using a regular (left) and an irregular (right) decomposition. High coefficients $E_2 = 1e+06$ are shown in dark purple in the picture, subdomains shown in different colors in the background and by half-transparent slices. Visualization for $N = 8$ and $H/h = 5$.

Composite material no. 2, regular partitioning, and $H/h = 10$											
	Algorithm Ia, Ib, and Ic					*Algorithm II*			*Algorithm III*		
N		κ	its	$\|U\|$	$\#\mathcal{E}_{evp}$	κ	its	$\|U\|$	κ	its	$\|U\|$
3^3	a)	**3.37**	15	2548	72 (57.1%)	**3.37**	15	2548	**3.55**	18	556
	b)	**3.37**	15	2548	0 (0%)						
	c)	**3.55**	18	556	0 (0%)						
4^3	a)	**3.36**	15	7332	216 (60%)	**3.36**	15	7332	**3.54**	18	1536
	b)	**3.36**	15	7332	0 (0%)						
	c)	**3.54**	18	1536	0 (0%)						
5^3	a)	**3.39**	15	15896	480 (61.5%)	**3.39**	15	15896	**3.55**	17	3272
	b)	**3.39**	15	15896	0 (0%)						
	c)	**3.55**	17	3272	0 (0%)						

Table 8.1: Compressible linear elasticity with $E_1 = 1$, $E_2 = 1e + 06$. Coarse spaces for TOL $= 10$ for all generalized eigenvalue problems. H is the size of the subdomains, i.e., $(1/H)^3$ is the number of subdomains, κ is the estimated condition number, 'its' is the number of PCG iterations, $|U|$ is the size of the adaptive coarse space, $\#\mathcal{E}_{evp}$ is the number of eigenvalue problems computed (and the percentage wrt. the total number of eigenvalue problems). Condition numbers below 50 are marked in bold face.

For all these test cases discarding the edge constraints from face eigenvalue problems never seems to be a good option and often results in nonconvergence ($its = 500$); but also for Algorithm II a large condition number and a large number of iterations are observed. On the other hand, our Algorithm Ia, which makes use of our new coarse space, in accordance with the theory, results in small condition numbers for all cases – while, compared to Algorithm II, adding around or fewer than 5% of additional constraints to the coarse space. Algorithms Ib and Ic can reduce the number of edge eigenvalue problems significantly, e.g., around 50%. However, for Algorithm Ib this still results in an almost identical coarse space. The coarse space of Algorithm Ic is always significantly smaller than the one of Algorithm Ib and Algorithm II. Nevertheless, condition number and iteration counts of Algorithm Ic are comparable to those of Algorithm Ia while Algorithm II cannot ensure this.

In general, for irregularly partitioned domains, we see that that the amount of edge eigenvalue problems is between 0% and 12% for Algorithm Ia while this can be reduced to 0 to 7% by Algorithms Ib and Ic. For Algorithm Ib, in the mean, we get

Composite material no. 1, irregular partitioning, and $H/h = 3$.											
	Algorithm Ia, Ib, and Ic					*Algorithm II*			*Algorithm III*		
N		κ	its	$\lvert U\rvert$	$\#\mathcal{E}_{evp}$	κ	its	$\lvert U\rvert$	κ	its	$\lvert U\rvert$
3^3	a)	**8.55**	30	93	7 (11.9%)	**8.55**	30	90	8.43e+05	56	50
	b)	**8.55**	30	93	4 (7.1%)						
	c)	**8.55**	31	84	4 (7.1%)						
5^3	a)	**14.48**	37	278	14 (5.2%)	**14.48**	37	264	3.35e+05	211	153
	b)	**14.48**	37	278	8 (3.0%)						
	c)	**14.48**	37	227	8 (3.0%)						
7^3	a)	**14.08**	40	605	48 (6.0%)	2.97e+05	118	569	3.00e+05	434	358
	b)	**14.08**	41	602	21 (2.7%)						
	c)	**14.08**	41	506	21 (2.7%)						
9^3	a)	**16.45**	42	1076	90 (5.2%)	3.61e+05	115	1029	4.76e+05	500	704
	b)	**16.45**	42	1075	45 (2.7%)						
	c)	**16.45**	42	932	45 (2.7%)						
11^3	a)	**15.87**	43	1774	167 (5.2%)	2.69e+05	190	1668	3.72e+05	500	1174
	b)	**15.87**	43	1770	95 (3.0%)						
	c)	**15.87**	43	1580	95 (3.0%)						
13^3	a)	**17.32**	45	3070	303 (5.6%)	2.79e+05	345	2911	3.42e+05	500	2032
	b)	**17.32**	45	3068	171 (3.3%)						
	c)	**17.32**	45	2753	171 (3.3%)						

Table 8.2: Compressible linear elasticity with $E_1 = 1$, $E_2 = 1e+06$. Coarse spaces for TOL $= 10$ for all generalized eigenvalue problems.

about 2% to 3% edge eigenvalue problems and, compared to Algorithm II, 1% to 2% additional constraints; see Tables 8.2, 8.3, and 8.4, and 8.5. There are also cases when Algorithm Ib and II coincide; see, e.g., Table 8.5.

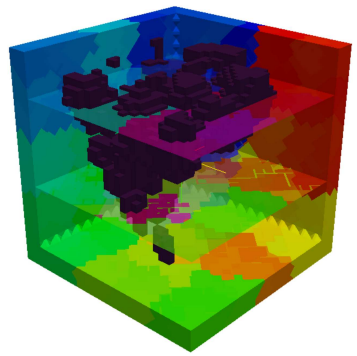

Figure 8.3: Coefficient distribution on a representative volume element (RVE). An irregular partitioning is used. High coefficients $E_2 = 1e+06$ are shown in dark purple, subdomains are shown in different colors in the background and by half-transparent slices.

For irregularly partitioned domains the computational overhead of Algorithm Ic, compared to the "classic" approach in Algorithm III, might be of up to 7% of extra eigenvalue problems and up to 2-3 times as many constraints but is then mostly mandatory for convergence and to reduce the condition number from $1e+05$ to 10; see, Tables 8.2, 8.3, and 8.4, and 8.5. However, compared to Algorithm II we can save up to 40% of the constraints by using Algorithm Ic.

We conclude that the additional edge eigenvalue problems and the resulting constraints are often necessary to obtain a small condition number and even mandatory if pcg is expected to converge in a small number of iterations. The only configurations when Algorithm III converged in fewer than 100 iterations were cases when coefficient jumps did not appear at subdomain edges, or in small examples with fewer subdomains, when the influence of the Dirichlet boundary was still strong.

Composite material no. 1, irregular partitioning, and $H/h = 6$.											
		Algorithm Ia, Ib, and Ic				*Algorithm II*			*Algorithm III*		
N		κ	its	$\|U\|$	$\#\mathcal{E}_{evp}$	κ	its	$\|U\|$	κ	its	$\|U\|$
3^3	a)	**8.70**	34	642	2 (2.0%)	**8.70**	34	642	1.37e+06	81	188
	b)	**8.70**	34	642	1 (1.0%)						
	c)	**8.72**	34	405	1 (1.0%)						
5^3	a)	**9.78**	36	3323	25 (4.2%)	**11.43**	36	3316	5.54e+05	213	924
	b)	**9.78**	36	3323	12 (2.1%)						
	c)	**10.62**	36	2092	12 (2.1%)						
7^3	a)	**10.91**	37	9388	65 (3.6%)	**10.91**	37	9350	1.22e+06	455	2672
	b)	**10.91**	37	9388	27 (1.5%)						
	c)	**13.48**	39	6308	27 (1.5%)						

Table 8.3: Compressible linear elasticity with $E_1 = 1$, $E_2 = 1e + 06$. Coarse spaces for TOL = 10 for all generalized eigenvalue problems.

Composite material no. 2, irregular partitioning and $H/h = 5$.											
		Algorithm Ia, Ib, and Ic				*Algorithm II*			*Algorithm III*		
N		κ	its	$\|U\|$	$\#\mathcal{E}_{evp}$	κ	its	$\|U\|$	κ	its	$\|U\|$
3^3	a)	**14.12**	37	1312	0 (0%)	**14.12**	37	1312	2.39e+05	463	523
	b)	**14.12**	37	1312	0 (0%)						
	c)	**14.12**	37	1114	0 (0%)						
5^3	a)	**13.91**	39	5675	23 (4.1%)	**13.91**	39	5639	5.46e+05	500	2261
	b)	**13.91**	39	5675	19 (3.5%)						
	c)	**13.92**	39	4840	19 (3.5%)						
7^3	a)	**14.58**	42	15250	89 (5.5%)	1.81e+05	84	15104	4.93e+05	500	6420
	b)	**14.58**	42	15250	70 (4.4%)						
	c)	**14.58**	42	13336	70 (4.4%)						
9^3	a)	**16.24**	43	32083	165 (4.6%)	6.74e+03	66	31897	3.16e+05	500	13591
	b)	**16.24**	43	32083	138 (3.9%)						
	c)	**16.24**	43	28372	138 (3.9%)						

Table 8.4: Compressible linear elasticity with $E_1 = 1$, $E_2 = 1e + 06$. Coarse spaces for TOL = 10 for all generalized eigenvalue problems.

Composite material no. 2, irregular partitioning and $H/h = 10$.											
		Algorithm Ia, Ib, and Ic				*Algorithm II*			*Algorithm III*		
N		κ	its	$\|U\|$	$\#\mathcal{E}_{evp}$	κ	its	$\|U\|$	κ	its	$\|U\|$
3^3	a)	**9.86**	35	4441	1 (1.0%)	**9.86**	35	4441	3.46e+05	243	1101
	b)	**9.86**	35	4441	0 (0%)						
	c)	**11.25**	36	3364	0 (0%)						
4^3	a)	**9.60**	35	10524	0 (0%)	**9.60**	35	10524	8.88e+05	379	2583
	b)	**9.60**	35	10524	0 (0%)						
	c)	**11.57**	37	7417	0 (0%)						
5^3	a)	**9.90**	36	22704	13 (2.0%)	**9.90**	36	22704	1.04e+06	500	5490
	b)	**9.90**	36	22704	2 (0.3%)						
	c)	**11.12**	37	17219	2 (0.3%)						

Table 8.5: Compressible linear elasticity with $E_1 = 1$, $E_2 = 1e + 06$. Coarse spaces for TOL = 10 for all generalized eigenvalue problems.

Representative Volume Element with $E_1 = 210$, $E_2 = 210000$, regular and irregular partitioning, $N = 8^3$ and $H/h = 4$.											
	Algorithm Ia, Ib, and Ic					*Algorithm II*			*Algorithm III*		
part.		κ	its	$\lvert U\rvert$	$\#\mathcal{E}_{evp}$	κ	its	$\lvert U\rvert$	κ	its	$\lvert U\rvert$
reg.	a)	**10.04**	34	5950	2352 (63.6%)	**10.04**	35	5246	244.60	80	1066
	b)	**10.04**	34	5950	736 (35.4%)						
	c)	**10.06**	34	4769	736 (35.4%)						
irreg.	a)	**13.97**	37	700	114 (5.6%)	**13.97**	37	689	361.85	98	344
	b)	**13.97**	37	700	27 (1.4%)						
	c)	**13.97**	38	579	27 (1.4%)						

Table 8.6: Compressible linear elasticity. Coarse spaces for TOL = 10 for all generalized eigenvalue problems.

8.2. Steel microstructure. In this section, we will consider a representative volume element (RVE) representing the microstructure of a modern steel; see Figure 8.3.

The RVE has been obtained from the one in [42, Fig. 5.5] by resampling; see also the discussion below. As in [42], we use $\nu = 0.3$, $E_1 = 210$ and $E_2 = 210000$ as (artificial) material parameters. There, about 12% of the volume is covered by the high coefficient E_2. We have resampled the RVE from $64 \times 64 \times 64$ to $32 \times 32 \times 32$ voxels. Here, the coefficient was set to E_2 if at least three of the original voxels had a high coefficient. This procedure guarantees that the ratio of high and low coefficients is not changed.

We see from our results in Table 8.6 that Algorithms Ia, Ib, and II do behave quite the same. The amount of extra work for our modified coarse space in Algorithms Ia and Ib compared to Algorithm II is small. Algorithm Ic uses a reduced coarse space that still guarantees small condition numbers and convergence within a comparable number of pcg iterations while the smallest coarse space, represented by Algorithm III, gives larger condition numbers and iteration counts.

8.3. Randomly distributed coefficients. We turn towards randomly distributed coefficients and now perform 100 runs with different coefficients for every configuration. We consider a linear elastic and compressible material on a discretization of the unit cube, i.e., a structured fine mesh consisting of cubes each containing five tetrahedra. We enforce zero Dirichlet boundary conditions just for the face with $x = 0$ and zero Neumann boundary conditions elsewhere. We apply the volume force $f := [0.1, 0.1, 0.1]^T$. We have seen in the preceding examples that the coarse space of Algorithm Ib only differs to a minor degree or not at all from that of Algorithm Ia. In the conference proceedings [28, Table 2], it has been reported for heterogeneous diffusion problems with a random coefficient distribution that Algorithms Ia, Ib, and Ic all yield essentially the same results. The same holds for the case of linear elasticity with randomly distributed coefficients considered here. Therefore, we will restrict ourselves to present results for Algorithms Ib, II, and III in this section.

Besides N, we vary the number of tetrahedra with a high coefficient. We test a 50/50 and 20/80 ratio of high and low coefficients; see Figure 8.4. In Tables 8.7 and 8.8, we present the *arithmetic mean* $\overline{x}$, the *median* $\widetilde{x}$ and the *standard deviation* σ for different numbers N of subdomains with $H/h = 5$.

Again, we see that discarding the edge constraints resulting from face eigenvalue problems can result in large condition numbers and iteration counts; see the results for

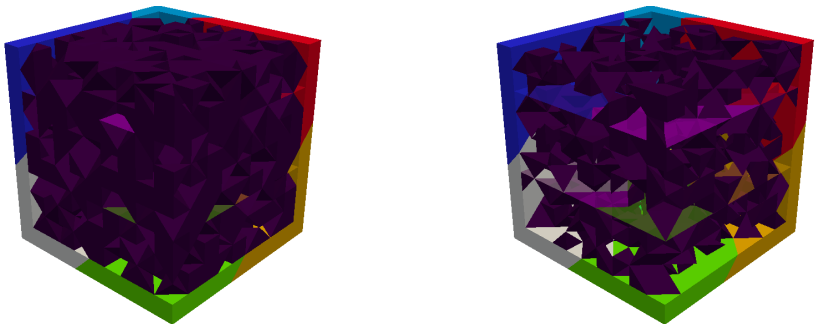

a) 50% high coefficients.

a) 20% high coefficients.

Figure 8.4: Randomly distributed coefficients on Ω with irregular partitioning. High coefficients ($\mathrm{E}_2 = 1e+06$) are shown in dark purple in the picture, subdomains shown in different colors in the background and by half-transparent slices; visualized for $N = 8$ and $H/h = 5$. We perform 100 runs for each setting.

Algorithm III in Tables 8.7 and 8.8. Nonetheless, keeping these edge constraints does, again, not always guarantee a small condition number and fast convergence, as the results for Algorithm II show. The number of extra eigenvalue problems for Algorithm Ib is either 0% or 4% for our examples. Since there are no egde eigenvalue problems for $N = 27$ subdomains Algorithm Ib and II coincide in that case. Moreover, since the edge eigenvalue problems always produce fewer than 1% of additional constraints the computational overhead for Algorithm Ib is quite moderate compared to Algorithm II; see Tables 8.7 and 8.8. As the median shows for $N \in \{64, 125\}$ in Table 8.7 and $N = 64$ in Table 8.8, the majority of problems is well solved by the coarse space of Algorithm II. However, the arithmetic mean points out that there are several problems with a high condition number if this coarse space is used. Let us just note that "several problems" for $N = 64$ subdomains and Table 8.8 even means 46 of 100 runs. Even worse, for $N = 125$ subdomains, Algorithm II exhibited in 21 and in 87 of 100 runs a condition number of at least $1e+04$, as well as in 21 and in 33 cases even a condition number of $1e+05$ or higher; see Tables 8.7 and 8.8.

We see that, by investing fewer than 1% of additional constraints resulting from our edge eigenvalue problems, our Algorithm Ib can guarantee a condition number around TOL. This shows that this additional amount of work is worthwile and can guarantee a small condition number and convergence within a reasonable number of pcg iterations.

8.4. Almost incompressible linear elasticity. In this section, we consider a linear elastic material which consists of compressible and almost incompressible parts. The compressible material parts have a Poisson ratio of $\nu = 0.3$ and for the almost incompressible parts we consider different values of Poisson's ratio with $0.45 \leq \nu < 0.5$. We also consider different distributions of Young's modulus in the material, allowing for large coefficient jumps. Let us note that such large coefficient jumps in Young's modulus and simultaneously letting Poisson's ratio ν almost approach the incompressible limit 0.5 for some parts of the material, can lead to very ill-conditioned local matrices $K_{BB}^{(i)}$.

As before, we consider the unit cube but we slightly increase the volume force $f =$

Randomly distributed coefficients with 50% high and 50% low coefficients, irregular partitioning, and $H/h = 5$.											
		Algorithm Ib				*Algorithm II*			*Algorithm III*		
N		κ	its	$\lvert U\rvert$	$\#\mathcal{E}_{evp}$	κ	its	$\lvert U\rvert$	κ	its	$\lvert U\rvert$
3^3	$\overline{x}$	**10.20**	35.17	180.94	0 (0%)	**10.20**	35.17	180.94	7.53e+05	135.06	59.65
	$\widetilde{x}$	**10.09**	35	179.5	0 (0%)	**10.09**	35	179.5	6.89e+05	134	59
	σ	0.68	0.67	24.12	-	0.68	0.66	24.12	2.19e+05	27.39	7.76
4^3	$\overline{x}$	**10.80**	36.09	383.77	9 (3.7%)	6.85e+04	37.52	382.58	1.02e+06	222.96	137.37
	$\widetilde{x}$	**10.53**	36	381	9 (3.7%)	**10.84**	36	380	1.01e+06	221	137
	σ	1.00	0.51	29.10	-	1.83e+05	3.74	29.01	2.31e+05	30.70	11.43
5^3	$\overline{x}$	**11.38**	36.70	721.46	23 (4.1%)	9.42e+05	39.35	719.27	8.54e+05	276.70	243.58
	$\widetilde{x}$	**11.13**	37	717	23 (4.1%)	**11.62**	37	717	8.12e+05	269.5	241.5
	σ	1.20	0.72	54.54	-	2.13e+05	5.64	54.47	1.90e+05	39.56	17.85

Table 8.7: Compressible linear elasticity with $\mathrm{E}_1 = 1$, $\mathrm{E}_2 = 1e+06$. Coarse spaces for TOL = 10 for all generalized eigenvalue problems.

Randomly distributed coefficients with 20% high and 80% low coefficients, irregular partitioning, and $H/h = 5$.											
		Algorithm Ib				*Algorithm II*			*Algorithm III*		
N		κ	its	$\lvert U\rvert$	$\#\mathcal{E}_{evp}$	κ	its	$\lvert U\rvert$	κ	its	$\lvert U\rvert$
3^3	$\overline{x}$	**8.40**	30.74	1311.94	0 (0%)	**8.40**	30.74	1311.94	3.89e+05	486.03	499.76
	$\widetilde{x}$	**8.38**	31	1311.5	0 (0%)	**8.38**	31	1311.5	3.78e+05	500	501
	σ	0.61	0.79	66.14	-	0.61	0.79	66.14	1.21e+05	24.67	33.36
4^3	$\overline{x}$	**9.01**	32.68	2680.69	9 (3.7%)	6.93e+04	39.58	2663.58	5.57e+05	500	1100.85
	$\widetilde{x}$	**9.04**	33	2678	9 (3.7%)	2.90e+03	38	2661.5	5.22e+05	500	1103
	σ	0.50	0.63	81.22	-	1.16e+05	8.04	81.16	1.85e+05	0	42.15
5^3	$\overline{x}$	**9.12**	32.96	6015.56	23 (4.1%)	9.39e+04	58.14	5969.77	4.98e+05	500	2360.64
	$\widetilde{x}$	**9.08**	33	6009	23 (4.1%)	7.12e+04	55	5959.5	4.62e+05	500	2359
	σ	0.56	0.61	148.91	-	9.33e+04	18.12	148.19	1.38e+05	0	70.92

Table 8.8: Compressible linear elasticity with $\mathrm{E}_1 = 1$, $\mathrm{E}_2 = 1e+06$. Coarse spaces for TOL = 10 for all generalized eigenvalue problems.

$[-1,-1,-1]^T$, pushing the domain towards the Dirichlet boundary. We use inf-sup stable $\mathcal{Q}_2-\mathcal{P}_0$ finite elements for both, the compressible and the almost incompressible parts. We present numerical results for three different material distributions.

In our first set of experiments, we consider a distribution of the Poisson ration in layers of ν_1 and ν_2. The layers have a thickness of two elements in x_3 direction. Here, ν_1 takes different values whereas $\nu_2 = 0.3$. We have $E = 1$ on the complete domain Ω. For all three algorithms, the condition numbers and iteration counts are uniformly bounded with respect to ν_2 approaching 0.5. All algorithms also yield condition numbers and iteration counts of a comparable size; see Table 8.9. For the material distributions considered in this example, Algorithm III seems to be sufficient.

The second example will be the composite material no. 2 from Section 8.1. Here, we use $\mathrm{E}_1 = 1$ and $\mathrm{E}_2 = 1e+03$. We consider a variable Poisson ratio $\nu_1 \in [0.3, 0.5)$ for all finite elements with $\mathrm{E}_1 = 1$ and a fixed Poisson ratio $\nu_2 = 0.3$ for those finite elements with $\mathrm{E}_2 = 1e+03$. Table 8.10 indicates uniformly bounded condition numbers and iteration counts for Algorithms Ia and II. For Algorithm III, the condition number and the iteration counts still seem to bounded but at a higher level. Algo-

Layered distribution of compressible and almost incompressible materials, irregular partitioning, $H/h = 5$, and $N = 4^3$.										
	Algorithm Ia				*Algorithm II*			*Algorithm III*		
ν_1	κ	its	$\|U\|$	$\#\mathcal{E}_{evp}$	κ	its	$\|U\|$	κ	its	$\|U\|$
0.45	**6.83**	27	3804	15 (4.8%)	**6.83**	27	3800	**7.72**	29	712
0.499	**7.11**	28	4042	15 (4.8%)	**7.11**	28	4038	**8.41**	31	757
0.49999	**7.12**	28	4051	15 (4.8%)	**7.12**	28	4047	**8.62**	31	759
0.4999999	**7.12**	28	4051	15 (4.8%)	**7.12**	28	4047	**8.62**	31	759
0.499999999	**7.12**	28	4051	15 (4.8%)	**7.12**	28	4047	**8.62**	32	759

Table 8.9: Almost incompressible linear elasticity with ν_1 as given, $\nu_2 = 0.3$, E = 1 constant. Coarse spaces for TOL = 10 for all generalized eigenvalue problems.

Composite material no. 2, irregular partitioning, $H/h = 5$, and $N = 4^3$.										
	Algorithm Ia				*Algorithm II*			*Algorithm III*		
ν_1	κ	its	$\|U\|$	$\#\mathcal{E}_{evp}$	κ	its	$\|U\|$	κ	its	$\|U\|$
0.45	**9.04**	31	6560	15 (4.8%)	**9.04**	31	6556	**12.27**	37	1239
0.499	**13.08**	34	7330	15 (4.8%)	**13.08**	34	7326	**34.71**	50	1402
0.49999	**8.84**	31	7571	15 (4.8%)	**8.84**	31	7564	589.80	98	1460
0.4999999	**8.80**	31	7576	15 (4.8%)	**8.80**	31	7569	796.50	106	1461
0.499999999	**8.80**	31	7576	15 (4.8%)	**8.80**	31	7569	799.90	120	1461

Table 8.10: Almost incompressible linear elasticity with ν_1 as given, $\nu_2 = 0.3$, $E_1 = 1$, $E_2 = 1e{+}03$. Coarse spaces for TOL = 10 for all generalized eigenvalue problems.

rithms Ia and II perform as in the compressible case but at the cost of a larger coarse space.

In our third set of experiments, we consider an almost incompressible material with both, ν and $E = 1$ constant on the complete domain. Table 8.11 shows that this becomes a hard problem for Algorithm III and also for Algorithm II. With ν approaching the incompressible limit, the condition number of the mentioned algorithms will be several magnitudes larger than this of Algorithm Ia. In contrast to the other algorithms, Algorithm Ia can guarantee a small condition number and an almost constant number of pcg iterations.

REMARK 3. *Note that the automatic coarse space constructed here for the almost incompressible case is slightly larger than the a priori coarse spaces constructed in [17] and [19], which introduce only a single (additional) constraint for each subdomain in 2D to cope with almost incompressible elasticity [17], or where all face constraints can be summed to a single constraint in 3D [19].*

8.5. Heuristic approach on reducing the number of eigenvalue problems and constraints based on the residual. We now consider the heuristic approach described in Section 7.3 to reduce the number of (edge) eigenvalue problems. We apply this approach to our Algorithm Ib for compressible elasticity and to Algorithm Ia for almost incompressible test problems. Note that this approach can equally be adopted for the coarse spaces of Algorithms Ic, II, or III. We report the number of eigenvalue problems solved and denoted by "$\#\text{EVP}_U$", as well the number of eigenvalue problems discarded by our heuristic approach of Section 7.3., denoted by "$\#\text{EVP}_{\text{disc\_S7.3}}$"; see Tables 8.12, 8.13, and 8.14. For the computation of the residual r (see Section 7.3), we simply use $\lambda = 0$. For the cases where Algorithm Ib was used, we also report the

Homogeneous material, irregular partitioning, $H/h = 5$, and $N = 4^3$.										
	Algorithm Ia				*Algorithm II*			*Algorithm III*		
ν	κ	its	$\lvert U\rvert$	$\#\mathcal{E}_{evp}$	κ	its	$\lvert U\rvert$	κ	its	$\lvert U\rvert$
0.45	**6.52**	27	4085	15 (4.8%)	**6.52**	27	4081	**7.69**	29	764
0.499	**7.34**	30	4736	15 (4.8%)	**7.34**	29	4732	**22.17**	43	892
0.49999	**6.81**	28	4909	15 (4.8%)	**12.18**	29	4900	1.98e+03	88	933
0.4999999	**6.81**	28	4913	15 (4.8%)	1.06e+03	38	4903	1.97e+05	119	934
0.499999999	**6.81**	28	4913	15 (4.8%)	1.06e+05	59	4903	1.97e+07	144	934

Table 8.11: Almost incompressible linear elasticity with ν as given, E = 1 constant. Coarse spaces for TOL = 10 for all generalized eigenvalue problems.

Composite material no. 1, irregular partitioning, and $H/h = 6$.							
$\tau_2 = 0.01, \tau_\infty = 10\tau_2$							
N	λ_{min}	λ_{max}	its	$\lvert U\rvert$	$\#\text{EVP}_U$	$\#\text{EVP}_{\text{disc\_S7.3}}$	$\#\text{EVP}_{\text{disc\_S7.1.2}}$
3^3	1	**8.79**	35	629	63	36	1
5^3	1	**15.71**	40	3229	312	267	13
7^3	1	120.10	72	9095	937	812	38
$\tau_2 = 0.001, \tau_\infty = 10\tau_2$							
N	λ_{min}	λ_{max}	its	$\lvert U\rvert$	$\#\text{EVP}_U$	$\#\text{EVP}_{\text{disc\_S7.3}}$	$\#\text{EVP}_{\text{disc\_S7.1.2}}$
3^3	1	**8.79**	35	632	64	35	1
5^3	1	**10.63**	37	3260	326	253	13
7^3	1	**15.50**	40	9269	998	751	38

Table 8.12: Compressible linear elasticity with $\text{E}_1 = 1$, $\text{E}_2 = 1e+06$. Coarse space of **Algorithm Ib** with heuristically reduced number of eigenvalue problems according to Section 7.3 using TOL = 10 for all generalized eigenvalue problems. For the results without heuristic of Section 7.3, see Table 8.3.

number of (edge) eigenvalue problems discarded by this algorithm as $\#\text{EVP}_{\text{disc\_S7.1.2}}$; cf. Section 7.1.2. In this section, we report λ_{min} and λ_{max} instead of κ.

We also consider different values of τ_2, namely $\tau_2 \in \{0.01, 0.001\}$, each with $\tau_\infty = 10\tau_2$. Using a larger value of τ_2, e.g., setting $\tau_2 = 0.1$, does not give acceptable results anymore in about half of our test cases. We refrain from reporting the details here.

The choice $\tau_\infty = 10\tau_2$ is heuristic and motivated from initial testing. The use of τ_∞ and τ_2 is motivated by the fact that localized high peaks and widespread heterogeneities with a (10 times) lower value should both trigger the adaptivity.

For our composite material no. 1 we observe good or acceptable behavior of our heuristics, and up to roughly 50% of the eigenvalue problems are saved; see Table 8.12. Nevertheless, to keep the condition number at the order of TOL, we have to use $\tau_2 = 0.001$.

We again turn towards randomly distributed cofficients which turned out to be the most challenging problem in the previous sections. For the corresponding Table 8.13, we additionally report that with $\tau_2 = 0.001$ the condition number was low in all runs, and the iteration number did not exceed 40. The heuristics thus worked well. However, Algorithm Ib was identical to Algorithm Ia in 99 of 100 cases for the randomized coefficients, since they are highly oscillatory, i.e., in this setting, it is very likely that heterogeneities are present at all edges.

From our results in Table 8.14 we see that we can save a substantial number

Randomly distributed coefficients with 20% high and 80% low coefficients, irregular partitioning, and $H/h = 5$.								
$\tau_2 = 0.001, \tau_\infty = 10\tau_2$								
N		λ_{min}	λ_{max}	its	$\lvert U\rvert$	$\#\text{EVP}_U$	$\#\text{EVP}_{\text{disc\_S7.3}}$	$\#\text{EVP}_{\text{disc\_S7.1.2}}$
5^3	$\overline{x}$	1	**9.16**	32.97	6010.63	530.42	24.57	0.01
	$\widetilde{x}$	1	**9.09**	33	6005	530.5	24.5	0
	σ	0	0.55	0.64	149.97	4.35	4.33	0.10

Table 8.13: Compressible linear elasticity with $\text{E}_1 = 1$, $\text{E}_2 = 1e+06$. Coarse space of **Algorithm Ib** with heuristically reduced number of eigenvalue problems according to Section 7.3 using TOL = 10 for all generalized eigenvalue problems. For the results without heuristic of Section 7.3, see Table 8.8.

Composite material no. 2, irregular partitioning, $H/h = 5$, and $N = 4^3$.						
$\tau_2 = 0.01, \tau_\infty = 10\tau_2$						
ν_1	λ_{min}	λ_{max}	its	$\lvert U\rvert$	$\#\text{EVP}_U$	$\#\text{EVP}_{\text{disc\_S7.3}}$
0.45	1	**30.09**	55	4038	93	217
0.499	1	67.27	56	6535	253	57
0.49999	1	**37.98**	50	6988	272	38
0.4999999	1	**38.00**	50	6993	272	38

Table 8.14: Almost incompressible linear elasticity with variable ν_1 as given, $\nu_2 = 0.3$, $\text{E}_1 = 1$, $\text{E}_2 = 1e+03$. Coarse space of **Algorithm Ia** with heuristically reduced number of eigenvalue problems according to Section 7.3 using TOL = 10 for all generalized eigenvalue problems. For the results without heuristic of Section 7.3, see Table 8.10.

of eigenvalue problems when ν is still far away from the incompressible limit. As ν approaches the limit the computational savings are more modest.

8.6. Efficiently solving the eigenvalue problems. The numerical solution of the eigenvalue problems can be expensive but their "exact" solution is required by the current theory. Additionally, the construction of the operators of the eigenvalue problem can also be expensive if an eigensolver is used that needs the matrices in explicit form.

However, an approximation of the extreme eigenvectors by an iterative method is sufficient in practice. This was already reported to be successful for adaptive BDDC using LOBPCG; see [56]. In Tables 8.15 and 8.16, we show results for $H/h = 15$ using an iterative eigenvalue problem solver. We use an implementation of LOBPCG (see [41, 40]) with block size 10, preconditioned by a Cholesky decomposition of the right hand side of the eigenvalue problem. We conduct a given number of maximum iterations as indicated in the tables. If the smallest computed eigenvalue of the considered block exceeds the tolerance TOL, we proceed with another pass of the algorithm and search for 10 new eigenvectors in a subspace orthogonal to the previously computed eigenvector approximations. All approximate eigenvectors corresponding to approximate eigenvalues above TOL will be added to the coarse space.

In Table 8.15, we consider a variable number of subdomains $N \in \{3^3, 4^3, 5^3\}$ and use a single iteration of LOBPCG. This already seems to work acceptably. For $N = 3^3$ subdomains, we also consider different values for the maximum iteration count, i.e., $\{1, 2, 5, 10, 200\}$ and with a requested tolerance for convergence of the LOBPCG solver of $1e-5$; see Table 8.16. We see that, in terms of resulting FETI-DP iterations, exceeding a number of 5 LOBPCG iterations does not seem to be worthwhile. Note that the METIS decomposition for $N = 3^3$ subdomains here does not lead to any edge eigenvalue problem. Therefore, Algorithm Ia, Ib and II behave identically.

Composite material no. 1, irregular partitioning, and $H/h = 15$.											
	Algorithm Ia, Ib, and Ic					*Algorithm II*			*Algorithm III*		
N		κ	its	$\lvert U\rvert$	$\#\mathcal{E}_{evp}$	κ	its	$\lvert U\rvert$	κ	its	$\lvert U\rvert$
3^3	a)	**26.74**	50	2360	0 (0%)	**26.74**	50	2360	8.028e+05	150	462
	b)	**26.74**	50	2360	0 (0%)						
	c)	**26.77**	50	1228	0 (0%)						
4^3	a)	**28.37**	54	4472	2 (0.7%)	**28.37**	54	4472	4.315e+05	215	863
	b)	**28.37**	54	4472	0 (0%)						
	c)	**28.39**	55	1962	0 (0%)						
5^3	a)	**43.87**	61	10178	8 (1.2%)	**43.87**	61	10178	6.86e+05	288	1941
	b)	**43.87**	61	10178	0 (0%)						
	c)	**43.93**	62	5334	0 (0%)						

Table 8.15: Compressible linear elasticity with $\mathrm{E}_1 = 1$, $\mathrm{E}_2 = 1e+06$. Coarse spaces for $\mathrm{TOL} = 10$ for all generalized eigenvalue problems. Solution of the local eigenvalue problems by LOBPCG with 1 iteration.

Composite material no. 1, irregular partitioning, $N = 3^3$ and $H/h = 15$.											
	Algorithm Ia, Ib, and Ic					*Algorithm II*			*Algorithm III*		
LOBPCG max. its		κ	its	$\lvert U\rvert$	$\#\mathcal{E}_{evp}$	κ	its	$\lvert U\rvert$	κ	its	$\lvert U\rvert$
1	a)	**26.74**	50	2360	0 (0%)	**26.74**	50	2360	8.03e+05	150	462
	b)	**26.74**	50	2360	0 (0%)						
	c)	**26.77**	50	1228	0 (0%)						
2	a)	**17.65**	41	2623	0 (0%)	**17.65**	41	2623	7.76e+05	123	505
	b)	**17.65**	41	2623	0 (0%)						
	c)	**17.65**	42	1322	0 (0%)						
5	a)	**10.04**	37	2762	0 (0%)	**10.04**	37	2762	7.71e+05	126	531
	b)	**10.04**	37	2762	0 (0%)						
	c)	**12.86**	38	1374	0 (0%)						
10	a)	**12.61**	38	2782	0 (0%)	**12.61**	38	2782	7.70e+05	128	541
	b)	**12.61**	38	2782	0 (0%)						
	c)	**12.85**	40	1396	0 (0%)						
200	a)	**11.55**	38	3108	0 (0%)	**11.72**	38	3108	7.70e+05	113	686
	b)	**11.55**	38	3108	0 (0%)						
	b)	**12.86**	38	1665	0 (0%)						

Table 8.16: Compressible linear elasticity with $\mathrm{E}_1 = 1$, $\mathrm{E}_2 = 1e+06$. Coarse spaces for $\mathrm{TOL} = 10$ for all generalized eigenvalue problems. Solution of the local eigenvalue problems by LOBPCG with indicated number of maximum iterations.

9. Conclusion. We have presented an adaptive coarse space approach for FETI-DP methods (Algorithm Ia) including a condition number bound for general coefficient jumps inside subdomains and across subdomain boundaries as well as almost incompressible elasticity in 3D. The bound only depends on geometrical constants and a prescribed tolerance from local eigenvalue problems. Our approach is based on the classic adaptive approach from [44] but we use a small number (fewer than 5 percent) of additional edge eigenvalue problems. Our experiments support our theory and show that the new method is able to cope with situations where the classic approach fails. Moreover, we have given two techniques on how to reduce the number of eigenvalue problems and constraints from Algorithm Ia which work very well, i.e., Algorithm Ib and Ic. We have seen in our numerical experiments that the classic coarse space of [44] (Algorithm III) can be sufficient if coefficient jumps do only occur

at subdomain faces. However, if jumps are present across or along subdomain edges, in general, neither a small condition number nor a low count of Krylov iterations (or even convergence) can be guaranteed by Algorithm III, which does not use any edge constraints. For difficult coefficient distributions, at least the edge constraints resulting from face eigenvalue problems should be added to the coarse space. The resulting approach (Algorithm II) then can cope with a larger number of test problems. However, only Algorithms Ia, Ib, and Ic have been able to guarantee a low condition number for all our test cases. Although only Algorithm Ia is covered by our provable bound, Algorithm Ib performs almost identically. Algorithm Ic performs still comparably but can also save a considerable number of constraints; e.g., up to 40%. In simple cases, where Algorithm III is already successful, Algorithm Ic indeed reduces to Algorithm III. Moreover, our experiments show that the condition number can quite precisely be controlled by the tolerance TOL even if the reduction strategies of Section 7.1.2 (Algorithm Ib) or, additionally, Section 7.2 are used (Algorithm Ic). For our problems from almost incompressible elasticity, among Algorithms Ia, II, and III, only Algorithm Ia performed well for all our test problems. For regular decompositions, the number of edge eigenvalue problems in Algorithm Ia is quite high, but can be reduced considerably by switching to Algorithms Ib and Ic. For irregular decompositions, which is the more relevant case, the number of additional edge eigenvalue problems to be computed by Algorithm Ia is often only in a low single-digit percentage range and can further be reduced by switching to Algorithm Ib and Ic. Compared to Algorithm II, the number of additional constraints in Algorithm Ia and Ib is typically small, i.e., for our test problems, the mean is only between 1% to 3% of additional constraints. Moreover, compared to Algorithm II, Algorithm Ic reduces the number of edge constraints from face eigenvalue problems. Comparing the computational overhead of Algorithms Ia, Ib, and Ic to Algorithm III is in some way difficult since the additional constraints are mostly necessary to obtain convergence. Considering the computational overhead for the solution of the eigenvalue problems, we also showed that already an application of an iterative eigenproblem solver with just a few iterations results in a robust coarse space. Our heuristic strategy to reduce the number of eigenvalue problems (see Section 7.3) can save a substantial amount of computational work but requires some tuning of tolerances. In our numerical experiments, selecting a tolerance $0.001 \leq \tau_2 \leq 0.01$ with $\tau_\infty = 10\tau_2$ saved work while keeping the algorithm stable and reliable.

Acknowledgements. The use of the CHEOPS computing resources at the regional computing center (RRZK) of the University of Cologne is greatfully acknowledged.

REFERENCES

[1] Lourenço Beirão da Veiga, Luca F. Pavarino, Simone Scacchi, Olof B. Widlund, and Stefano Zampini, *Isogeometric BDDC preconditioners with deluxe scaling*, SIAM J. Sci. Comput., 36 (2014), pp. A1118–A1139.

[2] ———, *Adaptive selection of primal constraints for isogeometric BDDC deluxe preconditioners*, tech. report, Courant Institute, New York University, TR2015-977, 2015.

[3] Adi Ben-Israel and Thomas N. E. Greville, *Generalized inverses*, CMS Books in Mathematics/Ouvrages de Mathématiques de la SMC, 15, Springer-Verlag, New York, second ed., 2003. Theory and applications.

[4] Petter Bjørstad, Jacko Koster, and Piotr Krzyzanowski, *Domain decomposition solvers for large scale industrial finite element problems*, in Applied Parallel Computing. New

Paradigms for HPC in Industry and Academia, vol. 1947 of Lecture Notes in Comput. Sci., Springer, Berlin, 2001, pp. 373–383.

[5] Petter Bjørstad and Piotr Krzyzanowski, *A flexible 2-level Neumann-Neumann method for structural analysis problems*, in Parallel Processing and Applied Mathematics, vol. 2328 of Lecture Notes in Comput. Sci., Springer, Berlin, 2002, pp. 387–394.

[6] Juan G. Calvo and Olof B. Widlund, *An adaptive choice of primal constraints for BDDC domain decomposition algorithms*, tech. report, Courant Institute, New York University, TR2015-979, 2015.

[7] Clark Dohrmann and Clemens Pechstein, *In C. Pechstein, Modern domain decomposition solvers - BDDC, deluxe scaling, and an algebraic approach*, Slides to a talk at NuMa Seminar, JKU Linz, December 10th, 2013, http://people.ricam.oeaw.ac.at/c.pechstein/pechstein-bddc2013.pdf, (2013).

[8] Clark R. Dohrmann, *Robust constraint selection in BDDC algorithms for three-dimensional problems*. Talk at the 23rd International Conference on Domain Decomposition Methods in Science and Engineerung, Jeju Island, South Korea, July 5-10, 2015.

[9] Victorita Dolean, Frédéric Nataf, Robert Scheichl, and Nicole Spillane, *Analysis of a two-level Schwarz method with coarse spaces based on local Dirichlet-to-Neumann maps*, Comput. Methods Appl. Math., 12 (2012), pp. 391–414.

[10] Zdeněk Dostál, *Conjugate gradient method with preconditioning by projector*, International Journal of Computer Mathematics, 23 (1988), pp. 315–323.

[11] ———, *Projector preconditioning and domain decomposition methods*, Applied Mathematics and Computation, 37 (1990), pp. 75–81.

[12] Yalchin Efendiev, Juan Galvis, Raytcho Lazarov, and Joerg Willems, *Robust domain decomposition preconditioners for abstract symmetric positive definite bilinear forms*, ESAIM Math. Model. Numer. Anal., 46 (2012), pp. 1175–1199.

[13] Charbel Farhat, Michel Lesoinne, Patrick LeTallec, Kendall Pierson, and Daniel Rixen, *FETI-DP: a dual-primal unified FETI method. I. A faster alternative to the two-level FETI method*, Internat. J. Numer. Methods Engrg., 50 (2001), pp. 1523–1544.

[14] Charbel Farhat, Michael Lesoinne, and Kendall Pierson, *A scalable dual-primal domain decomposition method*, Numer. Linear Algebra Appl., 7 (2000), pp. 687–714. Preconditioning techniques for large sparse matrix problems in industrial applications (Minneapolis, MN, 1999).

[15] Juan Galvis and Yalchin Efendiev, *Domain decomposition preconditioners for multiscale flows in high-contrast media*, Multiscale Model. Simul., 8 (2010), pp. 1461–1483.

[16] ———, *Domain decomposition preconditioners for multiscale flows in high contrast media: reduced dimension coarse spaces*, Multiscale Model. Simul., 8 (2010), pp. 1621–1644.

[17] Sabrina Gippert, *Domain Decomposition Methods for Elastic Materials with Compressible and Almost Incompressible Components*, PhD thesis, Universität Duisburg-Essen, 2012.

[18] Sabrina Gippert, Axel Klawonn, and Oliver Rheinbach, *Analysis of FETI-DP and BDDC for linear elasticity in 3D with almost incompressible components and varying coefficients inside subdomains*, SIAM J. Numer. Anal., 50 (2012), pp. 2208–2236.

[19] ———, *A deflation based coarse space in dual-primal feti methods for almost incompressible elasticity*, in Numerical Mathematics and Advanced Applications - ENUMATH 2013, Assyr Abdulle, Simone Deparis, Daniel Kressner, Fabio Nobile, and Marco Picasso, eds., vol. 103 of Lecture Notes in Computational Science and Engineering, Springer International Publishing, 2015, pp. 573–581.

[20] Paulo Goldfeld, Luca F. Pavarino, and Olof B. Widlund, *Balancing Neumann-Neumann preconditioners for mixed approximations of heterogeneous problems in linear elasticity*, Numerische Mathematik, 95 (2003), pp. 283–324.

[21] Pierre Gosselet, Christian Rey, and Daniel J Rixen, *On the initial estimate of interface forces in FETI methods*, Comput. Methods Appl. Mech. Eng., 192 (2003), pp. 2749–2764.

[22] Marta Jarošová, Axel Klawonn, and Oliver Rheinbach, *Projector preconditioning and transformation of basis in FETI-DP algorithms for contact problems*, Math. Comput. Simulation, 82 (2012), pp. 1894–1907.

[23] George Karypis and Vipin Kumar, *A fast and high quality multilevel scheme for partitioning irregular graphs*, SIAM J. Sci. Comput., 20 (1998), pp. 359–392.

[24] Hyea Hyun Kim, *BDDC and FETI-DP methods with enriched coarse spaces for elliptic problems with oscillatory and high contrast coefficients*. Talk at the 23rd International Conference on Domain Decomposition Methods in Science and Engineerung, Jeju Island, South Korea, July 5-10, 2015.

[25] Hyea Hyun Kim, Eric Chung, and Junxian Wang, *BDDC and FETI-DP algorithms with adaptive coarse spaces for three-dimensional elliptic problems with oscillatory and high*

contrast coefficients, ArXiv e-prints, (June 24, 2016).

[26] Hyea Hyun Kim and Eric T. Chung, *A BDDC algorithm with enriched coarse spaces for two-dimensional elliptic problems with oscillatory and high contrast coefficients*, Multiscale Model. Simul., 13 (2015), pp. 571–593.

[27] Axel Klawonn, Martin Kühn, Patrick Radtke, and Oliver Rheinbach, *On three different approaches to adaptive coarse spaces for FETI-DP methods in 2D and on one approach in 3D*. Talk at the 23rd International Conference on Domain Decomposition Methods in Science and Engineerung, Jeju Island, South Korea, July 5-10, 2015.

[28] Axel Klawonn, Martin Kühn, and Oliver Rheinbach, *Adaptive coarse spaces for FETI-DP in three dimensions with applications to heterogeneous diffusion problems*, Accepted for publication in Lecture Notes in Computational Science and Engineering, Springer International Publishing, 2016. Proceedings of the 23rd International Conference on Domain Decomposition Methods in Science and Engineerung, Jeju Island, South Korea, July 5-10, 2015; 8 p.

[29] ———, *Using local spectral information in domain decomposition methods – A brief overview in a nutshell*, (2016). Submitted to Proceedings in Applied Mathematics and Mechanics (PAMM), 05/2016.

[30] ———, *Adaptive coarse spaces for FETI-DP in three dimensions*, tech. report, Technische Universität Bergakademie Freiberg, Fakultät für Mathematik und Informatik, Preprint 2015-11, November 23, 2015. `http://tu-freiberg.de/fakult1/forschung/preprints`.

[31] Axel Klawonn, Patrick Radtke, and Oliver Rheinbach, *FETI-DP methods with an adaptive coarse space*, SIAM J. Numer. Anal., 53 (2015), pp. 297–320.

[32] ———, *A comparison of adaptive coarse spaces for iterative substructuring in two dimensions*, Electron. Trans. Numer. Anal., 45 (2016), pp. 75–106.

[33] ———, *A comparison of adaptive coarse spaces for iterative substructuring in two dimensions*, tech. report, Technische Universität Bergakademie Freiberg, Fakultät für Mathematik und Informatik, Preprint 2015-05, July 2, 2015. `http://tu-freiberg.de/fakult1/forschung/preprints`.

[34] Axel Klawonn and Oliver Rheinbach, *A parallel implementation of dual-primal FETI methods for three-dimensional linear elasticity using a transformation of basis*, SIAM J. Sci. Comput., 28 (2006), pp. 1886–1906.

[35] ———, *Robust FETI-DP methods for heterogeneous three dimensional elasticity problems*, Comput. Methods Appl. Mech. Engrg., 196 (2007), pp. 1400–1414.

[36] ———, *Deflation, projector preconditioning, and balancing in iterative substructuring methods: connections and new results*, SIAM J. Sci. Comput., 34 (2012), pp. A459–A484.

[37] Axel Klawonn and Olof B. Widlund, *FETI and Neumann-Neumann iterative substructuring methods: connections and new results*, Comm. Pure Appl. Math., 54 (2001), pp. 57–90.

[38] ———, *Dual-primal FETI methods for linear elasticity*, Communications on Pure and Applied Mathematics, 59 (2006), pp. 1523–1572.

[39] Axel Klawonn, Olof B. Widlund, and Maksymilian Dryja, *Dual-Primal FETI Methods with Face Constraints*, in Recent Developments in Domain Decomposition Methods, Luca F. Pavarino and Andrea Toselli, eds., vol. 23 of Lecture Notes in Computational Science and Engineering, Springer, Berlin Heidelberg, 2002, pp. 27–40.

[40] Andrew V. Knyazev, *Toward the optimal preconditioned eigensolver: Locally optimal block preconditioned conjugate gradient method; MATLAB implementation*. `https://www.mathworks.com/matlabcentral/fileexchange/48-lobpcg-m`, Accessed: 2015-12-09.

[41] ———, *Toward the optimal preconditioned eigensolver: Locally optimal block preconditioned conjugate gradient method*, SIAM J. Sci. Comput., 23 (2001), pp. 517–541.

[42] Martin Lanser, *Nonlinear FETI-DP and BDDC Methods*, PhD thesis, Universität zu Köln, 2015.

[43] Jing Li and Olof B. Widlund, *FETI-DP, BDDC, and block Cholesky methods*, International Journal for Numerical Methods in Engineering, 66 (2006), pp. 250–271.

[44] Jan Mandel and Bedřich Sousedík, *Adaptive selection of face coarse degrees of freedom in the BDDC and the FETI-DP iterative substructuring methods*, Comput. Methods Appl. Mech. Engrg., 196 (2007), pp. 1389–1399.

[45] Jan Mandel, Bedřich Sousedík, and Jakub Šístek, *Adaptive BDDC in three dimensions*, Math. Comput. Simulation, 82 (2012), pp. 1812–1831.

[46] Reinhard Nabben and Cornelis Vuik, *A comparison of deflation and the balancing preconditioner*, SIAM J. Sci. Comput., 27 (2006), pp. 1742–1759.

[47] Roy A. Nicolaides, *Deflation of conjugate gradients with applications to boundary value problems*, SIAM J. Numer. Anal., 24 (1987), pp. 355–365.

[48] Duk-Soon Oh, Olof B. Widlund, Stefano Zampini, and Clark R. Dohrmann, *BDDC algorithms with deluxe scaling and adaptive selection of primal constraints for Raviart-Thomas vector fields*, tech. report, Courant Institute, New York University, TR2015-978, 2015.

[49] Clemens Pechstein and Clark R. Dohrmann, *A unified framework for adaptive BDDC*, tech. report, Johann Radon Institute for Computational and Applied Mathematics, Austrian Academy of Scienes (ÖAW), RICAM-Report 2016-20, 2016.

[50] Clemens Pechstein and Robert Scheichl, *Analysis of FETI methods for multiscale PDEs. Part II: interface variation*, Numer. Math., 118 (2011), pp. 485–529.

[51] Patrick Radtke, *Adaptive coarse spaces for FETI-DP and BDDC methods*, PhD thesis, Universität zu Köln, 2015.

[52] Oliver Rheinbach, *Parallel scalable iterative substructuring: Robust exact and inexact FETI-DP methods with applications to elasticity*, PhD thesis, Universität Duisburg-Essen, 2006.

[53] Daniel J. Rixen and Charbel Farhat, *A simple and efficient extension of a class of substructure based preconditioners to heterogeneous structural mechanics problems*, Internat. J. Numer. Methods Engrg., 44 (1999), pp. 489–516.

[54] Marcus V. Sarkis Martins, *Schwarz preconditioners for elliptic problems with discontinuous coefficients using conforming and non-conforming elements*, PhD thesis, New York University, 1994.

[55] Bedřich Sousedík, *Comparison of some domain decomposition methods*, PhD thesis, Czech Technical University in Prague, 2008.

[56] ———, *Adaptive-Multilevel BDDC*, PhD thesis, University of Colorado Denver, 2010.

[57] Bedřich Sousedík, Jakub Šístek, and Jan Mandel, *Adaptive-multilevel BDDC and its parallel implementation*, Computing, 95 (2013), pp. 1087–1119.

[58] Nicole Spillane, *An Adaptive MultiPreconditioned Conjugate Gradient Algorithm*, SIAM J. Sci. Comput., 38 (2016), pp. A1896–A1918.

[59] Nicole Spillane, Victorita Dolean, Patrice Hauret, Frédéric Nataf, Clemens Pechstein, and Robert Scheichl, *A robust two-level domain decomposition preconditioner for systems of PDEs*, Comptes Rendus Mathematique, 349 (2011), pp. 1255 – 1259.

[60] ———, *Abstract robust coarse spaces for systems of PDEs via generalized eigenproblems in the overlaps*, Numer. Math., 126 (2014), pp. 741–770.

[61] Nicole Spillane and Daniel J. Rixen, *Automatic spectral coarse spaces for robust finite element tearing and interconnecting and balanced domain decomposition algorithms*, Internat. J. Numer. Methods Engrg., 95 (2013), pp. 953–990.

[62] Andrea Toselli and Olof B. Widlund, *Domain Decomposition Methods - Algorithms and Theory*, vol. 34 of Springer Series in Computational Mathematics, Springer-Verlag, Berlin Heidelberg New York, 2005.

[63] Olof B. Widlund, *BDDC algorithms with adaptive choices of the primal constraints.* Talk at the 23rd International Conference on Domain Decomposition Methods in Science and Engineerung, Jeju Island, South Korea, July 5-10, 2015.